

2005

# Modification of CT quality assurance phantom for PET/CT alignment and PET resolution

Prashanth K. Nookala

*Louisiana State University and Agricultural and Mechanical College, pnooka1@lsu.edu*

Follow this and additional works at: [https://digitalcommons.lsu.edu/gradschool\\_theses](https://digitalcommons.lsu.edu/gradschool_theses)



Part of the [Physical Sciences and Mathematics Commons](#)

---

## Recommended Citation

Nookala, Prashanth K., "Modification of CT quality assurance phantom for PET/CT alignment and PET resolution" (2005). *LSU Master's Theses*. 4202.

[https://digitalcommons.lsu.edu/gradschool\\_theses/4202](https://digitalcommons.lsu.edu/gradschool_theses/4202)

This Thesis is brought to you for free and open access by the Graduate School at LSU Digital Commons. It has been accepted for inclusion in LSU Master's Theses by an authorized graduate school editor of LSU Digital Commons. For more information, please contact [gradetd@lsu.edu](mailto:gradetd@lsu.edu).

**MODIFICATION OF CT QUALITY ASSURANCE PHANTOM FOR  
PET/CT ALIGNMENT AND PET RESOLUTION**

**A Thesis**

**Submitted to the Graduate Faculty of the  
Louisiana State University and  
Agricultural and Mechanical College  
in partial fulfillment of the  
requirements for the degree of  
Master of Science**

**in**

**The Department of Physics and Astronomy**

**by  
Prashanth K Nookala  
B.Tech., Jawaharlal Nehru Technological University, 2001  
May 2005**

# ACKNOWLEDGEMENTS

It is a pleasure to thank the many people who made this thesis possible. I thank my advisor, Dr. Kenneth L Matthews II, for spending his valuable time to teach and guide me, without whom this work would not have been possible. I sincerely thank him for his suggestions and patience in motivating and nurturing me throughout this program.

I thank Dr. Oscar Hidalgo for his thoughts in shaping my thesis and his guidance during rotation at Mary Bird Perkins Cancer Center (MBPCC). I am grateful to Dr. Erno Sajo for his encouragement and support through out this program. I thank my committee members, Dr. John Gibbons and Dr. John Wefel for their valuable time and expertise to evaluate my thesis.

The guidance of Dr. William Bice and Dr. Sheldon Johnson was invaluable during clinical rotation at MBPCC. I also thank LSU and MBPCC Medical Physics faculty and staff for their support and making the course of study a memorable one.

Thanks to all my friends and colleagues in the Physics department, for providing me with an encouraging and competitive environment and support for my work.

There are countless other people whose names and faces pass through my mind as I ruminate about this period at LSU. So, I would have to include all of them saying that it was really a pleasure knowing them and that aspect, as much as anything else, made this whole journey worthwhile. I am thankful to all my friends and well wishers for their support in terms of providing congenial surroundings and making my stay at LSU memorable and enjoyable.

I thank my parents, brothers and other family members back in India, for being there in my hard times and for their encouragement, constant support, love and blessings without which I would not be here.

I also thank Department of Physics and Astronomy for supporting me financially by granting assistantships through out the course of study.

# TABLE OF CONTENTS

ACKNOWLEDGEMENTS .....	ii
LIST OF TABLES .....	vi
LIST OF FIGURES .....	viii
ABSTRACT .....	xii
CHAPTER 1. INTRODUCTION .....	1
1.1 Objectives .....	2
1.2 Hypothesis.....	3
CHAPTER 2. BACKGROUND PHYSICS.....	5
2.1 Computed Tomography (CT) .....	5
2.2 Positron Emission Tomography (PET) .....	7
2.3 PET/CT Dual Modality.....	9
2.4 Image Registration .....	11
CHAPTER 3. MATERIALS .....	14
3.1 ACR CT Accreditation Phantom, Gammex 464.....	14
3.2 Modified ACR CT Accreditation Phantom, Gammex 464.....	15
3.3 Inserts for Modified ACR CT Accreditation Phantom.....	15
3.4 Triple-line Insert for Deluxe SPECT Phantom.....	16
3.5 Hot Sphere Phantom .....	17
CHAPTER 4. METHODS .....	19
4.1 CT Quality Assurance.....	19
4.2 PET/CT Alignment Testing .....	19
4.2.1 Image Acquisition.....	19
4.2.2 PET/CT Image Analysis .....	20
4.3 Determination of PET Resolution.....	28
CHAPTER 5. RESULTS .....	29
5.1 CT Quality Assurance.....	29
5.1.1 CT Number Calibration .....	29
5.1.2 Slice Thickness .....	31
5.1.3 Low Contrast Resolution .....	32
5.1.4 High Contrast Resolution.....	36
5.1.5 Uniformity.....	36
5.2 PET/CT Alignment Tests.....	38
5.2.1 Results from Manual Method .....	38
5.2.2 Results from Maximum-Pixel Value Method.....	45
5.2.3 Results from Curve-fitting Method.....	52

5.2.4 Summary of PET/CT Alignment Test Results.....	57
5.3 PET Resolution.....	63
CHAPTER 6. SUMMARY AND CONCLUSIONS.....	66
REFERENCES.....	70
APPENDIX A IDL PROGRAMS FOR MANUAL METHOD.....	72
APPENDIX B IDL PROGRAMS FOR MAXIMUM-PIXEL VALUE METHOD.....	73
APPENDIX C IDL PROGRAMS FOR CURVE-FITTING METHOD.....	77
VITA.....	85

# LIST OF TABLES

Table 1: Specifications for Gammex 464 phantom .....	15
Table 2: Specifications for Triple-line Insert for Deluxe SPECT phantom.....	17
Table 3: Specifications for spheres of Hot Sphere phantom.....	18
Table 4: CT acquisition and display parameters to perform CT number calibration as given in the instruction manual using the Gammex phantom .....	30
Table 5: Acceptable CT number ranges for the Gammex phantom, specified by the ACR .....	30
Table 6: CT acquisition and display parameters to determine slice thickness using Gammex phantom.....	33
Table 7: CT acquisition and display parameters to determine low contrast resolution using Gammex phantom .....	34
Table 8: Low contrast resolution performed using Routine Head technique with the Gammex phantoms .....	35
Table 9: Low contrast resolution performed using Adult Abdomen technique with the Gammex phantoms .....	35
Table 10: CT acquisition parameters used to measure high contrast resolution.....	36
Table 11: High contrast resolution measured using High Resolution Chest technique and Adult Abdomen technique .....	37
Table 12: CT acquisition and display parameters to determine the uniformity using the Gammex phantom.....	37
Table 13: Measured PET/CT alignment errors for the modified Gammex phantom with acrylic insert using the Manual method.....	39
Table 14: Measured PET/CT alignment errors for the modified Gammex phantom with solid water insert using the Manual method .....	40
Table 15: Measured PET/CT alignment errors for the triple line source phantom using the Manual method .....	41
Table 16: Measured PET/CT alignment errors for the triple line source phantom rotated by 45° using the Manual method.....	42

Table 17: Measured PET/CT alignment errors for the hot sphere phantom using the Manual method .....	45
Table 18: Measured PET/CT alignment errors for the modified Gammex phantom with acrylic insert using the Maximum-pixel value method .....	46
Table 19: Measured PET/CT alignment errors for the modified Gammex phantom with solid water insert using the Maximum-pixel value method.....	47
Table 20: Measured PET/CT alignment errors for the triple line source phantom using the Maximum-pixel value method.....	48
Table 21: Measured PET/CT alignment errors for the triple line source phantom rotated by 45° using the Maximum-pixel value method .....	49
Table 22: Measured PET/CT alignment errors for the hot sphere phantom using the Maximum-pixel value method.....	52
Table 23: Measured PET/CT alignment errors for the modified Gammex phantom with acrylic insert using the Curve-fitting method .....	53
Table 24: Measured PET/CT alignment errors values for the modified Gammex phantom with solid water insert using the Curve-fitting method .....	54
Table 25: Measured PET/CT alignment errors for the triple line source phantom using the Curve-fitting method.....	55
Table 26: Measured PET/CT alignment errors for the triple line source phantom rotated by 45° using the Curve-fitting method .....	56
Table 27: Measured PET/CT alignment errors for the hot sphere phantom using the Curve-fitting method.....	59
Table 28: Average measured object size for different phantoms using the Curve-fitting method to determine the resolution.....	65
Table 29: Results obtained for different CT parameters using the three CT QA phantoms.....	67

# LIST OF FIGURES

Figure 1: Different types of CT scanner systems: (a) one ring system, (b) single slice, helical system, (c) multi detector system, (d) multi slice helical.....	7
Figure 2: Principle of annihilation coincidence detection of 511 keV photons.....	8
Figure 3: Illustrations of (a) scattered coincidence event, (b) random or multiple coincidence event and (c) true coincidence event. Each detected gamma ray is a single event.....	9
Figure 4: PET/CT showing dimensions and components for a GE Discovery ST.....	11
Figure 5: Photograph of the modified Gammex phantom, showing the location of insert holes and the inserts used for this research. Also, the four materials of different densities (bone, acrylic, polyethylene and air) in module 1 of the Gammex phantom can be seen, as can the acrylic and solid water inserts used for holding the radioactive isotopes .....	16
Figure 6: (a) Triple-line phantom and (b) Triple-line phantom mounted inside the ECT cylinder.....	17
Figure 7: Hot Sphere phantom comprising hollow sphere set.....	18
Figure 8: Screenshot showing the IDL 5.6 Student Edition graphical user interface and one PET slice of the Triple-line Source phantom.....	22
Figure 9: Screenshot showing points selected on either side of object for drawing profiles .....	22
Figure 10: Screenshot displaying the profile of the selected object on the resized PET image.....	23
Figure 11: Screenshot showing a CT slice of the Triple-line Source phantom .....	23
Figure 12: Screenshot showing the line for drawing a profile across the object on the CT image.....	24
Figure 13: Screenshot displaying the profile of the selected object on the CT image.....	24
Figure 14: Illustration of the Maximum-Pixel Value method using (a) PET image of a Triple-line Source phantom and (b) the profile of the object in the PET image of the Triple-line Source phantom .....	26

Figure 15: Illustration of the Maximum-Pixel Value method using (a) CT image of a Triple-line Source phantom and (b) the profile of the object in the CT image of the Triple-line Source phantom .....	26
Figure 16: CT image of the modified Gammex phantom with acrylic insert displaying different materials of different densities used for CT number calibration .....	30
Figure 17: CT number calibration for the different materials of the unmodified Gammex phantom and the modified Gammex phantom with either solid water or acrylic insert. The materials are (a) polyethylene, (b) bone, (c) acrylic, (d) air and (e) water.....	31
Figure 18: CT image of the modified Gammex phantom with acrylic insert showing the 0.5 mm wires used in determination of slice thickness .....	33
Figure 19: Slice thickness measured at constant 120 kVp setting. The specified acquisition slice thicknesses were 2.5 mm, 5 mm, and 7.5 mm .....	33
Figure 20: CT number of water measured for a constant slice thickness as a function of kVp setting for (a) 80 kVp, (b) 100 kVp, (c) 120 kVp, and (d) 140 kVp .....	34
Figure 21: CT image at S40 location illustrating determination of low contrast resolution (a) without region of interests (ROI) shown and (b) with ROIs shown.....	35
Figure 22: CT image of Module 4 of the modified Gammex phantom with acrylic insert illustrating determination of high contrast resolution at (a) a soft tissue window level, and (b) the recommended window level .....	37
Figure 23: (a) Uniformity measured with the modified and unmodified Gammex phantom, and (b) CT image of the modified Gammex phantom with acrylic insert at location S80 illustrating placement of center and edge regions of interest (ROI) for uniformity measurement .....	38
Figure 24: Measured center coordinates using the Manual method for the modified Gammex phantom with acrylic insert.....	39
Figure 25: Measured center coordinates using the Manual method for the modified Gammex phantom with solid water insert .....	40
Figure 26: Measured center coordinates using the Manual method for the triple line source phantom without rotation for (a) first source and (b) second source .....	41
Figure 27: Measured center coordinates using the Manual method for the triple line source phantom rotated by 45° for (a) first source and (b) second source .....	43

Figure 28: Measured center coordinates using the Manual method for the hot sphere phantom for (a) 18 mm diameter sphere, (b) 12 mm diameter sphere, (c) 6 mm diameter sphere, and (d) 8 mm diameter sphere.....	44
Figure 29: Measured center coordinates using the Maximum-Pixel Value method for the modified Gammex phantom with acrylic insert.....	46
Figure 30: Measured center coordinates using the Maximum-Pixel Value method for the modified Gammex phantom with solid water insert.....	47
Figure 31: Measured center coordinates using the Maximum-Pixel Value method for the triple line source phantom without rotation for (a) first source and (b) second source.....	48
Figure 32: Measured center coordinates using the Maximum-Pixel Value method for the triple line source phantom rotated by 45° for (a) first source and (b) second source.....	50
Figure 33: Measured center coordinates using the Maximum-Pixel Value method for the hot sphere phantom for (a) 18 mm diameter sphere, (b) 12 mm diameter sphere, (c) 6 mm diameter sphere, and (d) 8 mm diameter sphere.....	51
Figure 34: Measured center coordinates using the Curve-fitting method for the modified Gammex phantom with acrylic insert .....	53
Figure 35: Measured center coordinates using the Curve-fitting method for the modified Gammex phantom with solid water insert.....	54
Figure 36: Measured center coordinates using the Curve-fitting method for the triple line source phantom without rotation for (a) first source and (b) second source.....	55
Figure 37: Measured center coordinates using the Curve-fitting method for the triple line source phantom rotated by 45° for (a) first source and (b) second source ..	57
Figure 38: Measured center coordinates using the Curve-fitting method for the hot sphere phantom for (a) 18 mm diameter sphere, (b) 12 mm diameter sphere, (c) 6 mm diameter sphere, and (d) 8 mm diameter sphere .....	58
Figure 39: Measured alignment errors for the modified Gammex phantom with acrylic insert using (a) the Manual method, (b) the Maximum-Pixel Value method, and (c) the Curve-fitting method .....	60
Figure 40: Measured alignment errors for the modified Gammex phantom with solid water insert using (a) the Manual method, (b) the Maximum-Pixel Value method, and (c) the Curve-fitting method .....	61

Figure 41: Measured alignment errors for the Triple-line Source phantom using (a) the Manual method, (b) the Maximum-Pixel Value method, and (c) the Curve-fitting method.....62

Figure 42: Measured alignment errors for the Hot Sphere phantom using (a) the Manual method, (b) the Maximum-Pixel Value method, and (c) the Curve-fitting method.....63

Figure 43: Measured FWHM for (a) modified Gammex phantom with acrylic insert, (b) modified Gammex phantom with solid water insert, (c) triple line source phantom with center bars representing the line source at the center, and (d) hot sphere phantom with spheres of diameters 18 mm, 12 mm 6 mm and 8 mm respectively.....65

# ABSTRACT

Radiotherapy treatment planning utilizing PET and CT is rapidly gaining acceptance in oncology. A limiting factor of the dual modality is the PET/CT alignment. A small error in PET/CT alignment may result in giving large doses of radiation to healthy tissues as a result of poor treatment planning. For this purpose, regular quality assurance testing of PET/CT must be performed. Separate QA procedures and phantoms have been developed for the two different modalities. In particular, many existing phantoms cannot be used for both modalities, which is a requirement for evaluating PET/CT alignment. Our goal is to evaluate several existing phantom designs to evaluate their utility for checking PET/CT alignment. The three phantoms investigated are a Gammex 464 phantom, a Triple-Line Source PET phantom, and a Hot Sphere PET phantom. The PET phantoms are unmodified the Gammex 464 phantom is modified to perform PET/CT alignment. The Gammex 464 phantom is typically used for routine quality assurance of CT scanners. Several CT parameters are determined with this phantom before and after modification. Then PET/CT alignment testing is performed using this modified CT phantom and the two other phantoms. Three methods have been used for analyzing the PET/CT images to measure the PET/CT alignment errors. The methods are the Manual method which calculates the alignment error from hand-drawn profiles, the Maximum-Pixel Value method which measures the error based on the pixel value of the objects in the PET/CT images, and the Curve-fitting method, which measures the alignment error by getting the best fit values for the object profiles. The Curve-fitting method also estimates the PET resolution from apparent size of objects in the phantoms.

Our PET/CT alignment data and results suggest that the Maximum-Pixel Value method for the modified phantom with acrylic insert is a good choice for measuring the PET/CT alignment error, providing a reasonable balance between computational analysis effort and measurement precision.

# CHAPTER 1

## INTRODUCTION

Accurate, patient-specific anatomical information is a prerequisite for successful radiation therapy planning and delivery to the entire extent of tumor, while minimizing dose to normal tissues surrounding it. For this reason, imaging in radiation oncology is very important. Many advances in radiation oncology have resulted from improvements in imaging modalities like computed tomography (CT), magnetic resonance imaging (MRI) and positron emission tomography (PET).<sup>1</sup> CT is a morphologically oriented imaging method. Unlike CT, PET is a functionally oriented method. PET with an FDG tracer utilizes the mechanism of biochemical reactions inside the patient and uses coincidence detection of annihilation photons to determine the tumor position. Both the methods have advantages as well as limitations. CT provides high resolution imaging but has a difficulty in distinguishing between tumors and healthy tissues. PET is sensitive to small differences in metabolism between tumors and healthy tissues. However spatial resolution provided by PET is low. These limitations of CT and PET can be addressed by using the combination of both modalities; parallel display of the two modalities complements and confirms each other's results. Radiotherapy treatment planning utilizing PET and CT is rapidly gaining acceptance in oncology. A limiting factor of the dual modality is the PET/CT alignment. A small error in PET/CT alignment may result in giving large doses of radiation to healthy tissues and result in poor treatment planning. For this purpose, regular quality assurance testing of PET/CT must be performed.

Historically, separate QA procedures and phantoms have been developed for the two different modalities. In particular, many existing phantoms cannot be used for both modalities, and for evaluating PET/CT alignment, a single QA phantom for both the modalities is a requirement. Our goal is to evaluate several existing phantom designs to evaluate their utility for checking PET/CT alignment. Ideally, the phantom should also allow other PET or CT QA measurements to be performed. If an existing phantom is modified to allow alignment testing, the effect of this modification should be insignificant on its routine QA. The final product of this thesis is a recommendation of a phantom and analysis method for PET/CT alignment QA.

## **1.1 Objectives**

The main objectives of this research can be summarized as follows

- Evaluate several QA phantoms for PET/CT alignment
- Evaluate different methods for measuring PET/CT alignment

The three phantoms investigated are a Gammex 464 ACR CT accreditation phantom, a Triple-Line Source PET phantom, and a Hot Sphere PET phantom. A detailed explanation with figures for these phantoms is provided in Chapter 3. The PET phantoms are unmodified, but the Gammex 464 is modified to perform PET/CT alignment. The Gammex 464 phantom is typically used for routine quality assurance of CT scanners. This phantom is modified in such a way that it can be used for PET/CT alignment parallel to performing routine CT QA. For all three phantoms, the PET and CT images are analyzed using three different methods for locating the centers of objects. Alignment error is determined, and the results are compared among the three phantoms. Also, regular CT QA is performed using the modified Gammex phantom and compared with

that of the original phantom to check the impact of the modification on its performance. Finally the estimated spatial resolution for the PET scanner is reported, because this is a typical PET QC parameter and it is calculated automatically as part of the PET/CT alignment analysis.

The modification to the Gammex phantom involves creating a hole in the phantom in which a radioactive insert is placed. Two different insert materials are compared for this purpose, with  $^{18}\text{F}$  used as the radioactive source in both cases. Results show that modification of the phantom on regular CT QA performance has minimal effect. An important conclusion is that alignment error measured for PET/CT depends on the type of analysis method as well as the phantom used for locating objects in the images.

## **1.2 Hypothesis**

The hypothesis of this research can be summarized as follows

- The modified Gammex 464 CT QA phantom should allow assessment of PET/CT alignment, without altering the quality of CT QA results.
- The Triple-line Source phantom should provide the most reliable measurement of alignment error with all analysis methods.
- The Modified Gammex phantom should be most economical in terms of set up time and the range of tests that can be performed.
- The Hot sphere phantom will show any variation in the quality of the alignment error measurements and PET resolution as a function of object diameter..

In Chapter 2, the basic physics of CT, PET and PET/CT dual modality scanners is explained and current research relevant to PET/CT alignment is reviewed. In Chapter 3, a

description of materials used in this research is presented. In Chapter 4, the methods developed and used for this research are explained. In Chapter 5, results and discussions are provided while the conclusions of this research are given in Chapter 6.

# CHAPTER 2

## BACKGROUND PHYSICS

### 2.1 Computed Tomography (CT)

Computed tomography (CT) is an x-ray imaging technique used to visualize thin slices of the body. Sir Godfrey Hounsfield developed the first CT scanner in 1972 while Alan Cormack developed a mathematical technique to reconstruct images from x-ray projections. Computed tomography uses an x-ray source, collimation, a rotating gantry, a patient aperture, photon detectors, and a data acquisition system to collect the attenuated x-ray beam. A thin fan beam of x-rays of about 80-120 kVp is incident on the patient transversely and these transmitted x-rays are detected by an array of detectors.

The reconstruction algorithm of CT scanners takes the transmitted x-ray intensities as input data and produces an output matrix. Each element of the output matrix represents the reconstructed linear attenuation coefficient of a small volume of the object (volume is the product of pixel area and slice thickness). The linear attenuation coefficients are expressed as CT numbers.<sup>1</sup> CT numbers are reported in Hounsfield units (HU).

The typical range of CT numbers is 2000 HU wide, although some modern scanners utilize a greater range up to 4000 HU wide. Each number represents attenuation relative to water (Equation 1); the attenuation coefficient of water is  $\mu_w$  while the attenuation coefficient of the material of interest is  $\mu_t$ . The attenuation coefficient of different materials is energy dependent. A CT number of +1000 HU corresponds to strong attenuation and -1000 HU corresponds to no attenuation.

$$\text{CT number (HU)} = \frac{1000 * (\mu_t - \mu_w)}{\mu_w} \quad (\text{Equation 1})$$

The CT numbers are mapped to a grey scale or color display for visual interpretation. Because the human eye cannot distinguish among 2000 different shades of grey, only a limited range of CT numbers is displayed to allow the observer to interpret the image. Window level (WL) indicates typically the central HU of all the numbers while window width (WW) represents the range of HU being displayed.

Several types of modern CT designs are illustrated in Figure 1. Development of slip ring technology for CT scanners during the 1980's enabled the x-ray tube to rotate continuously in one direction around the patient. This led to the development of helical CT. Single ring and multi-detector CT systems are illustrated in Figure 1(a) and Figure 1(c) respectively. Figure 1(b) illustrates a single slice helical system while Figure 1(d) illustrates a multi-slice helical system. In helical CT, the patient table mechanically moves through the x-ray beam while the x-ray tube rotates continuously in one direction. With this technology, information is acquired rapidly as a continuous volume of slices which allows larger anatomical regions of the body to be imaged in a single breath hold. This reduces the possibility of artifacts caused by patient movement and this also reduces scanning time. Contrast media often are used to improve contrast between the tissues of the body. These contrast media mostly contain high atomic mass substances and hence increase the attenuation coefficient of the organ.<sup>2</sup>

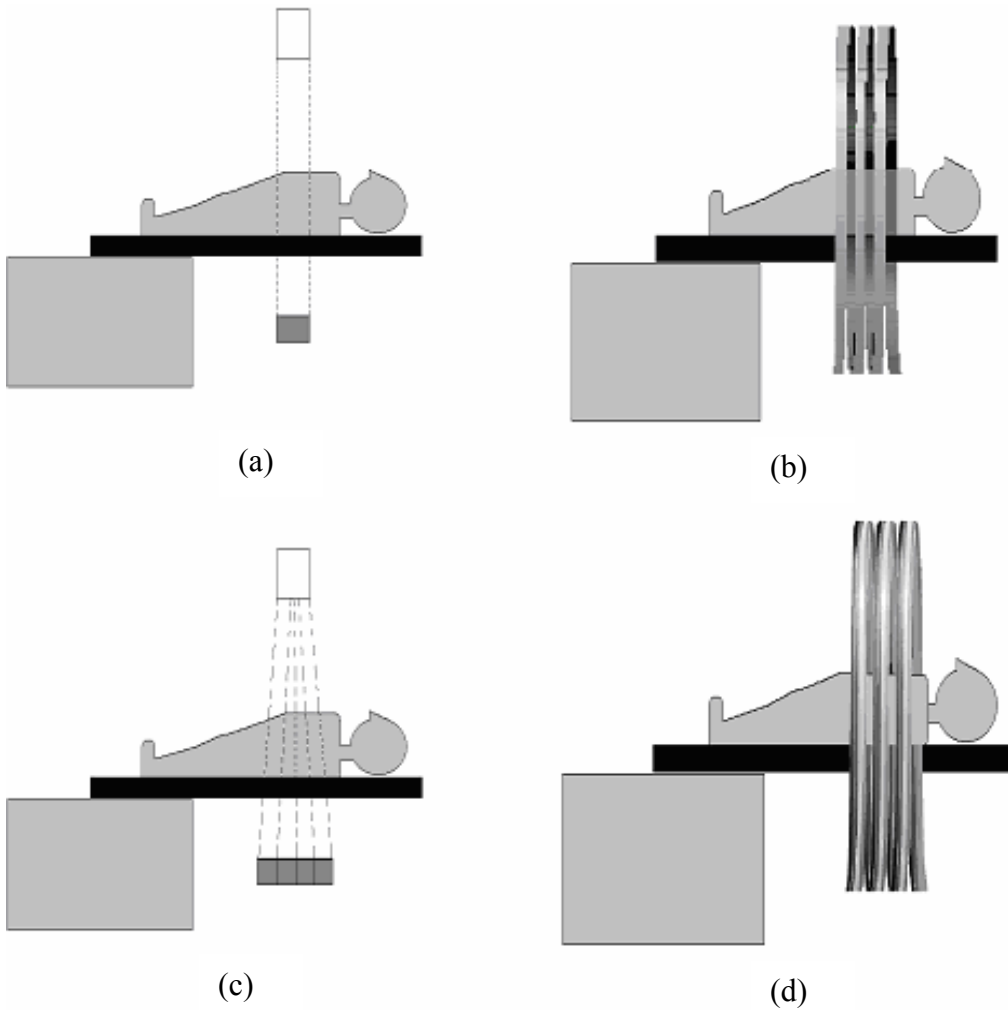


Figure 1: Different types of CT scanner systems: (a) one ring system, (b) single slice, helical system, (c) multi detector system, (d) multi slice helical.

## 2.2 Positron Emission Tomography (PET)

Positron emission tomography (PET) scanner design and performance have improved dramatically during the last decade. The first PET scanners were developed in the 1970's, though the first positron imaging started in the 1950's. The commercial production of PET scanners started in the mid 1980's. These scanners were limited to

small volumes, but improvements have continued with better resolution and larger fields of view. By the mid-1990's, PET had become an important diagnostic tool.<sup>3</sup>

PET makes use of the physical characteristics of radioisotopes that decay by positron emission. PET is based on the principle of annihilation coincidence detection (ACD) of two anti-collinear 511 keV photons which are products of annihilation of a positron and an electron. PET imaging is functional imaging. It is a method to measure metabolic processes, such as oxygen utilization and glucose metabolism.<sup>4</sup>

Figure 2 illustrates the basic principle of annihilation coincidence detection. An event is counted if two 511 keV photons generated from positron-electron annihilation are detected by the two detectors within a small timing interval,  $\tau$ .<sup>5</sup> Also, for the event to be regarded as valid, the subsequent line-of-response (LOR) formed between the detectors must be within the valid acceptance angle of the tomograph and the energy deposited in the detectors by both photons should be within a selected energy window.

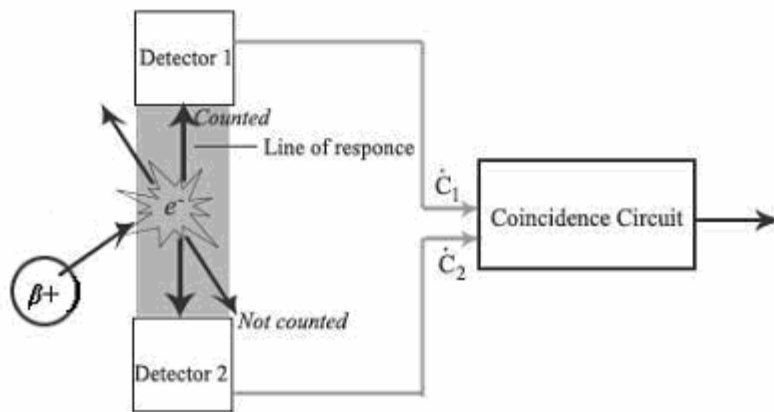


Figure 2: Principle of annihilation coincidence detection of 511 keV photons.

Detection events can be classified into five types (Figure 3). Single events are when a single photon is detected by one detector. A true coincidence event (Figure 3c) occurs when two photons from a single positron-electron annihilation are detected within the timing window. A random event (Figure 3b) occurs when two photons not arising from the same annihilation event are incident on the detectors within the coincidence time window of the system. Multiple events are similar to random events, and occur when three events from two annihilations are detected within the timing window. A scattered event (Figure 3a) occurs when at least one of the detected photons has undergone at least one Compton scattering event prior to detection.

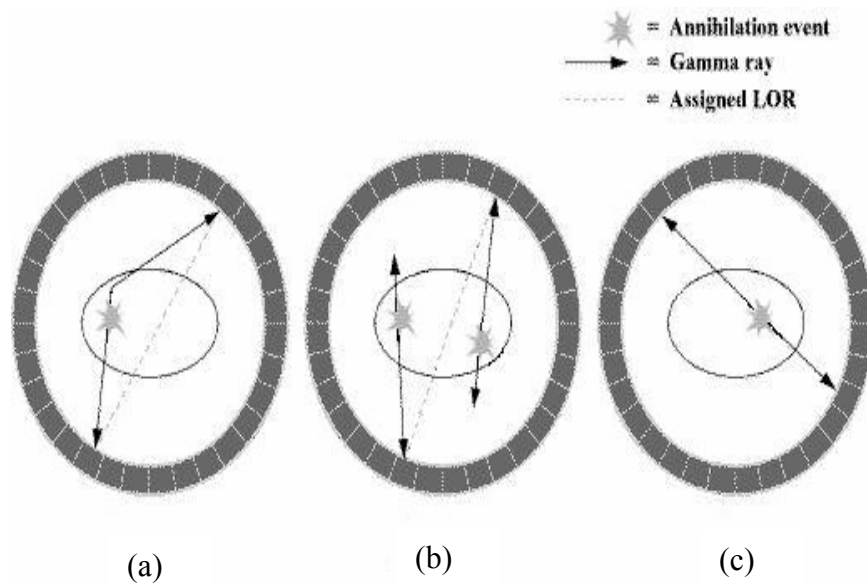


Figure 3: Illustrations of (a) scattered coincidence event, (b) random or multiple coincidence event and (c) true coincidence event. Each detected gamma ray is a single event.

## 2.3 PET/CT Dual Modality

One of the earliest dual-modality devices consisted of a scanner with combined anatomical (CT) and functional (single photon emission computed tomography [SPECT]) capabilities.<sup>6,7</sup> It used high-purity germanium as the detector for both modalities. The data

obtained from the CT images were also used to generate attenuation maps for correction of the SPECT data. The device allowed simultaneous emission-transmission acquisitions. This concept of a single device capable of performing both functional and anatomical imaging led to the development of novel hybrid imaging systems with a significant improvement in the accuracy of attenuation correction and co-registration. These systems allow for sequential acquisition of anatomic and functional data by combined transmission (using CT) and emission (using either PET, SPECT, or gamma camera-based coincidence detection) acquisitions during a single session.<sup>8</sup> SPECT/CT offers some advantages for imaging of small animals although PET/CT has generally been favored for clinical applications.<sup>9</sup>

Dual PET/CT scanners, along with the rapid growth of the clinical use of PET imaging have acquired an important role in oncologic imaging.<sup>10-12</sup> The combination of PET and CT scanning offers unique opportunities for oncology. PET/CT has the ability to provide a synergistic combination of PET and CT images, which could potentially be more valuable than the two exams performed separately. PET and CT are standard imaging tools that allow clinicians to diagnose and pinpoint the location of cancer within the body before making treatment recommendations. The highly sensitive PET scan picks up actively growing cancer cells (metabolism), and the CT scan provides a detailed picture of patient anatomy to reveal the size and shape of abnormal cancerous growths.

In PET/CT, the integration of the two modalities within a single gantry is straight forward when simultaneous operations of the CT and PET imaging systems are not required. Both the PET and CT components are mounted in the same gantry. Typically, CT is located in the front, with PET at the back as shown in Figure 4. The patient port is

typically 60-80 cm in diameter with an overall tunnel length of 110-160 cm and a 60-80 cm axial displacement between the center of the CT and the center of the PET imaging fields. A common patient bed is used for both modalities.

CT images are acquired and reconstructed, then transferred to the PET workstation to provide the attenuation correction factors required for reconstruction of the PET emission data. The PET and CT fused images are then displayed.<sup>13</sup> A study of clinical protocols for PET/CT scanning was done by Townsend, et al.<sup>14</sup> In his study, a detailed explanation is given of the process of preparing the patient for PET/CT scanning and the steps required for obtaining the PET and CT scans.

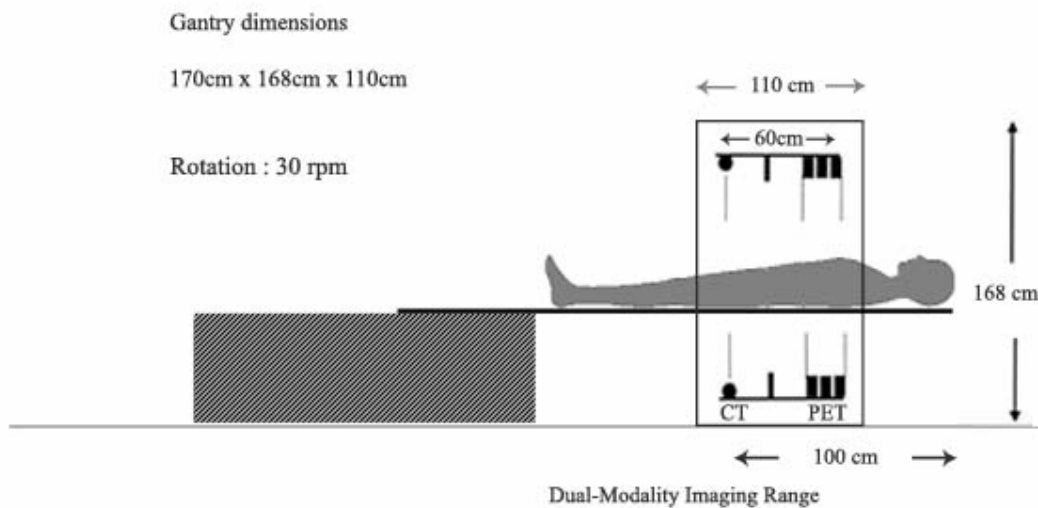


Figure 4: PET/CT showing dimensions and components for a GE Discovery ST.

## 2.4 Image Registration

The term image registration is most commonly used to denote the process of alignment of images and transforming them to a common coordinate system.<sup>15</sup> Image registration is also termed image fusion. Image fusion can augment the diagnostic

information obtained from functional studies in nuclear medicine. Registration of images can be performed using one of several methods. These include interactive registration, landmark-based registration, surface matching, maximization of mutual information, and elastic registration.

Fusion methods for separate functional and structural imaging data are usually based on extrinsic or intrinsic body markers.<sup>8</sup> External fiducial markers are attached to the body surface. These provide the required transformation if the markers are positioned identically for both studies. External markers are unsatisfactory for routine use because of the need for complex patient preparation and prospective planning; often, the studies are performed on different days, in different geographic locations, and using different types of imaging tables. Measurements based on surface points may not extrapolate well to points in the interior of the body. Internal anatomical landmarks eliminate the need for external fiducial markers and patient preparation. Reliable identification and accurate localization of these landmarks is, however, not always possible and requires considerable operator skill. These drawbacks are more prominent in nuclear medicine studies, which suffer from relatively low resolution.<sup>16</sup>

Inaccurate registration of separately acquired data may be due to differences in patient positioning between studies, as well as to differences in internal organ location, position, filling status, and volume at the time of imaging. Phantom validation to demonstrate methods for assessing the accuracy of PET/CT alignment has been studied by Lavelly, et al.<sup>17</sup> They have used the IAEA (International Atomic Energy Agency) brain phantom and an anthropomorphic head phantom for assessment of PET/CT image registration. In this study, comparison of structure-based registration with fiducial based

registration was performed and a target registration error was computed at each point in a three dimensional grid that spans the image volume.

Sequential acquisition of PET and CT data during a single imaging session can potentially eliminate many of the errors described with co-registration of independent studies and excludes the need for internal or external fiducial markers and complicated mathematical registration algorithms.<sup>12,18</sup> Alignment in dual PET/CT scanners is achieved with mechanical alignment of the PET and CT gantries, and also by using a common imaging table for both systems. A number of factors must be controlled to define reliable tumor treatment volume data in radiation oncology.<sup>19</sup> These factors are registration error, lack of uniformity of PET resolution over the field of view (FOV), and attenuation and scatter corrections applied to the PET data.

## **CHAPTER 3**

### **MATERIALS**

This chapter describes the phantoms used in this work. These phantoms are commercially available, but include some modifications. The applications of these phantoms, the specifications given by manufacturers, and the limitations of these phantoms are explained in this chapter. The three phantoms investigated are a Gammex 464 ACR CT accreditation phantom, a Triple-Line Source PET phantom, and a Hot Sphere PET phantom. The CT QA phantom, Gammex 464 is chosen for modification as it can be used for routine QA measuring many CT parameters other than the PET/CT alignment and PET resolution for which it is modified. Other phantoms are not selected for the modification as they can be used for testing of fewer QA parameters.

#### **3.1 ACR CT Accreditation Phantom, Gammex 464**

The ACR CT Accreditation phantom is used for initial CT quality assurance assessment and routine monthly CT QA testing; routine QA helps in providing required image quality. It is made of solid water, making this phantom a physically stable device that provides reproducible results over time.<sup>20</sup> This phantom is designed for evaluating CT parameters such as positioning accuracy, CT number accuracy, slice width, low contrast resolution, high contrast resolution, CT number uniformity and image noise. Table 1 details the specifications of this phantom.

Table 1: Specifications for Gammex 464 phantom

<b>Parameter</b>	<b>Value</b>
Number of modules	4
Depth of each module	4 cm
Diameter of each module	20 cm
Module material	Solid water
Module 1	CT number accuracy, slice thickness measurement
Module 2	Low contrast resolution measurement
Module 3	Uniformity measurement
Module 4	High contrast resolution measurement

### **3.2 Modified ACR CT Accreditation Phantom, Gammex 464**

The ACR CT Accreditation phantom was modified by making four cylindrical holes parallel to the cylinder axis. Two holes are visible in Figure 5. Two holes are in each end of the phantom. Each hole has a tight-fitting solid water plug of the same density as the phantom. All other specifications are the same as the unmodified Gammex phantom. For our experiments, we used only one of the cylindrical holes.

### **3.3 Inserts for Modified ACR CT Accreditation Phantom**

Cylindrical inserts were made for the modified ACR phantom of required dimensions to fit in the phantom holes. At the centre of each insert, we bored a cylindrical cavity of 8 mm diameter and 40 mm length for holding the radioactive material. The end of the cavity is threaded so that it can be plugged with a nylon screw. Inserts were made from two different materials to check if one material is easier to use. One insert is made of solid water while the other insert is made of acrylic.



Figure 5: Photograph of the modified Gammex phantom, showing the location of insert holes and the inserts used for this research. Also, the four materials of different densities (bone, acrylic, polyethylene and air) in module 1 of the Gammex phantom can be seen, as can the acrylic and solid water inserts used for holding the radioactive isotopes.

### **3.4 Triple-line Insert for Deluxe SPECT Phantom**

Figure 6 shows the Triple-line Insert in the Deluxe SPECT phantom manufactured by Data Spectrum Corporation. The three line inserts of this phantom are used to hold the radioactive material (FDG). It was originally designed to standardize the measurement of reconstructed spatial resolution of SPECT. The manufacturer also recommends it for assessment of PET/CT alignment.<sup>21</sup> This phantom can also be used for determination of PET spatial resolution in air or in water using an ECT cylinder (Figure 6b), for quantitative evaluation of reconstruction filters and scatter compensation methods and for research. Table 2 gives the specifications for this phantom.



Figure 6: (a) Triple-line phantom and (b) Triple-line phantom mounted inside the ECT cylinder.

Table 2: Specifications for Triple-line Insert for Deluxe SPECT phantom

Parameter	Value
Diameter of insert	18.6 cm
Diameter of line sources	~ 1 mm
Center to center spacing of line sources	7.5 cm
Useful height of line sources	7 cm
Location of the line sources	Center, 12 o'clock, 3 o'clock
Phantom material	acrylic

### 3.5 Hot Sphere Phantom

The Hot Sphere phantom comprises a set of hollow spheres (Figure 7) in the same outer water-filled cylinder used for the Triple-line Source phantoms. Similar to the Triple-line Source phantom, the Hot Sphere phantom is recommended to evaluate PET image quality and to assess PET/CT alignment.<sup>22</sup> This phantom is used for evaluation of spatial resolution, attenuation and scatter effects, evaluation of reconstruction methods, and research. Specifications for the spheres are given in Table 3.



Figure 7: Hot Sphere phantom comprising hollow sphere set.

Table 3: Specifications for spheres of Hot Sphere phantom

<b>Parameter</b>	<b>Outside diameter</b>	<b>Volume</b>	<b>Height of spheres above base plate to center</b>	<b>Wall thickness</b>	<b>Material</b>
Sphere 1	6 mm	0.031 mL	12.7 cm	1 mm	acrylic
Sphere 2	8 mm	0.125 mL	12.7 cm	1 mm	acrylic
Sphere 3	12 mm	0.5 mL	12.7 cm	1 mm	acrylic
Sphere 4	18 mm	2.0 mL	12.7 cm	1 mm	acrylic

# CHAPTER 4

## METHODS

### 4.1 CT Quality Assurance

The Gammex 464 ACR Accreditation phantom is a CT phantom designed to perform routine QA testing of CT scanners. It is made of four modules and each module is designed to check a set of CT parameters. The parameters that were studied in this project are CT number calibration, slice thickness, low contrast resolution, high contrast resolution and uniformity. All tests were performed following the instructions given in the Instruction Manual<sup>20</sup> for the ACR CT Accreditation Phantom.

In the CT scanner workstation, we created a protocol to execute the necessary image acquisitions for the different QA tests. Once the phantom is aligned with the laser lights of the scanner, the protocol is run to acquire the QA images. After the images are acquired, analysis to evaluate CT parameters is done following the procedure in the Instruction Manual.

### 4.2 PET/CT Alignment Testing

PET/CT alignment testing is performed on the three different phantoms, the modified Gammex 464, the Triple Line Source phantom, and the Hot Sphere phantom.

#### 4.2.1 Image Acquisition

Radioactive material ( $^{18}\text{F}$ -FDG) is placed in the Triple Line Source phantom, the acrylic insert and the solid water insert of the modified Gammex phantom, and the hollow spheres. Approximately 50  $\mu\text{Ci}$  is used in all phantoms but the concentrations are different because the phantoms have different volumes. Each phantom is positioned on

the PET/CT scanner and a CT scan is followed by a 4-minute 2D PET acquisition and a 3-minute 3D PET acquisition. The PET computer produces four different sets of reconstructed images for these scans. These are PET 2D acquisition with iterative reconstruction and measured attenuation correction (PET 2D IRMAC), PET 2D acquisition using iterative reconstruction without attenuation correction (PET 2D No AC), PET 3D acquisition with iterative reconstruction and measured attenuation correction (PET 3D IRMAC), and PET 3D acquisition using iterative reconstruction without measured attenuation correction (PET 3D No AC).

#### **4.2.2 PET/CT Image Analysis**

The PET/CT images obtained are analyzed using software IDL 5.6 Student Edition. Image analysis is performed using a manual method, a maximum-pixel value method and a curve-fitting method to measure the center co-ordinates of the objects in the images. In all three methods, the center co-ordinates of the objects in the CT images are compared with those of the PET images. The methods differ in the manner by which the center coordinates are extracted from the images. In the Manual method, the center coordinates are extracted by drawing profiles across the object. The Maximum-Pixel Value method uses a computer code written in IDL to determine the center coordinates of the markers based on their pixel values. The Curve-fitting method uses IDL's curve-fitting codes to extract the center coordinates of the markers.

##### **4.2.2.1 Manual Method**

This method manually determines the center co-ordinates of the objects in the PET and CT images. In this method, a CT or PET image is displayed and the user draws a profile across the approximate diameter of the object using an in-built profiling tool,

PROFILE, in IDL. The co-ordinates of the peak (for PET) or center (for CT) of the profile provide the center co-ordinate of the object.

The Manual method applied to PET images obtained from the Triple Line Source phantom is illustrated in Figure 8 through Figure 10. The image to be analyzed is displayed using the READ\_DICOM subroutine in IDL (Figure 8). To compare the center coordinates of the objects, both the PET and the CT images must have the same pixel size. The PET images are resized, or rebinned, using the CONGRID subroutine in IDL to produce the PET images of same pixel sizes as of the CT images. The PET images obtained after rebinning have more pixels because the FOV of the PET scanner is larger than that of the CT scanner. These excess pixels are cropped uniformly from all edges of the PET matrix to get the PET images to the same number of pixels as the CT images. Figure 9 shows a resized PET image from the Triple Line Source phantom with all three sources visible. Points are selected on either side of the object, across which the profile is desired (Figure 9). The PROFILE subroutine in IDL plots the profile between the selected points. The coordinates for the peak of the profile curve are determined, which gives the center coordinates of the selected object (Figure 10). The center coordinates of the source, which are given in pixel numbers, are converted to position in millimeters by multiplying by the pixel size.

To find the coordinates for the CT image, the same process is followed except that the CT image doesn't require rebinning and cropping. Also, the CT profiles are rectangle functions rather than Gaussian functions as in the PET profiles. The Manual method applied to CT images of the Triple Line Source phantom is illustrated in Figure 11 through Figure 13. To obtain the center coordinates of the object for the CT image, the

coordinates of the center of the rectangle profile (Figure 13) are added to the starting coordinates from where the profile is drawn, and the coordinates are converted to millimeters.

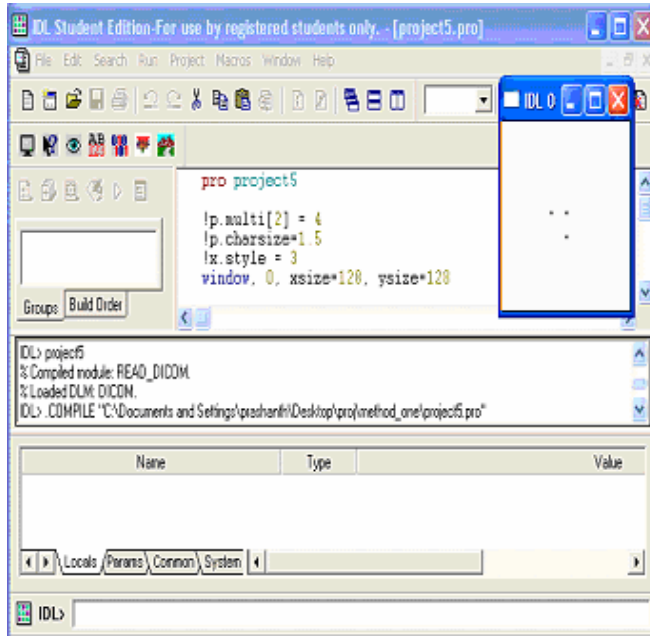


Figure 8: Screenshot showing the IDL 5.6 Student Edition graphical user interface and one PET slice of the Triple-line Source phantom.

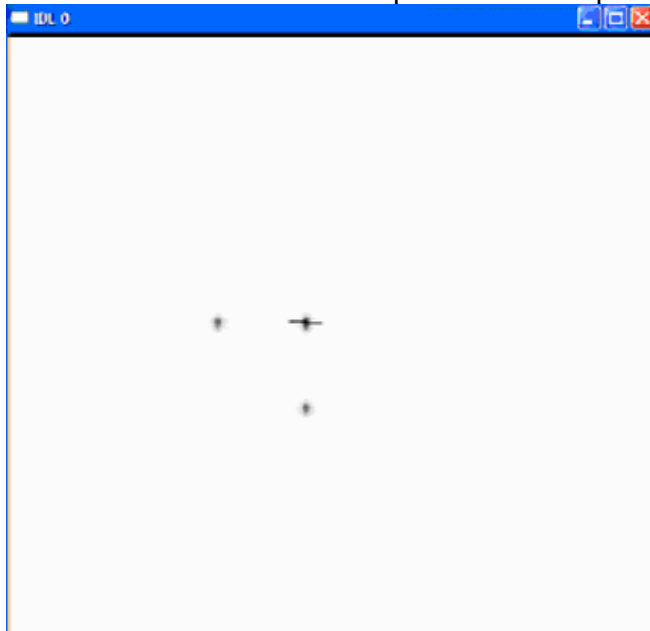


Figure 9: Screenshot showing points selected on either side of object for drawing profiles.

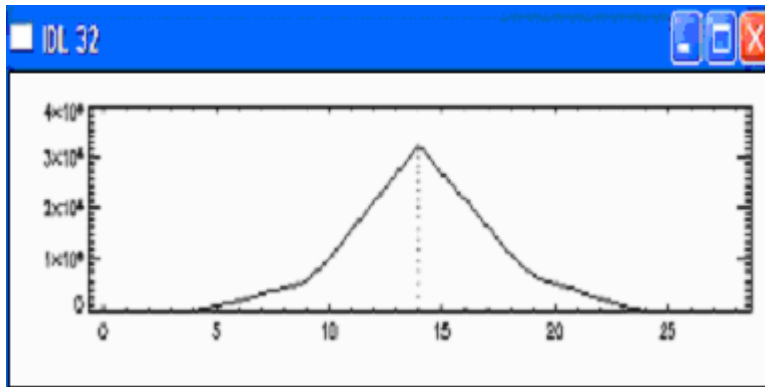


Figure 10: Screenshot displaying the profile of the selected object on the resized PET image.

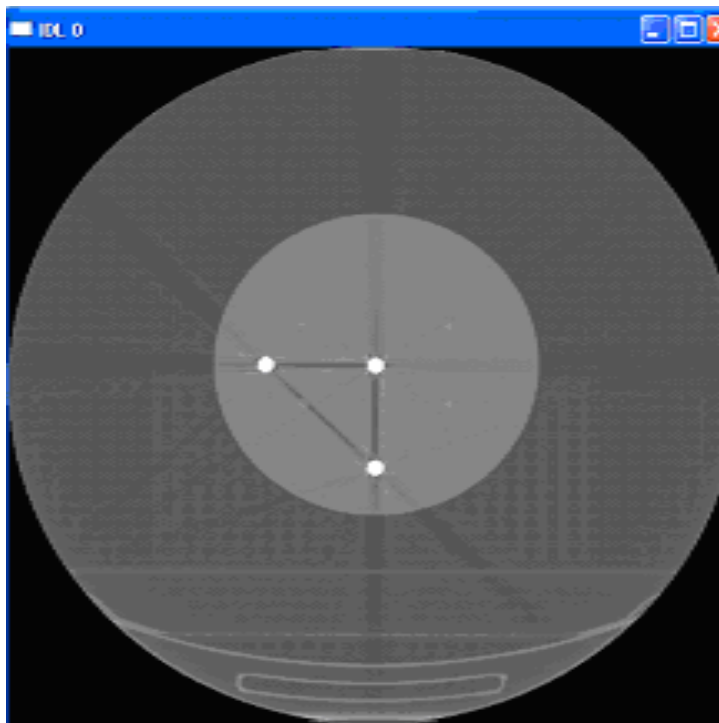


Figure 11: Screenshot showing a CT slice of the Triple-line Source phantom.

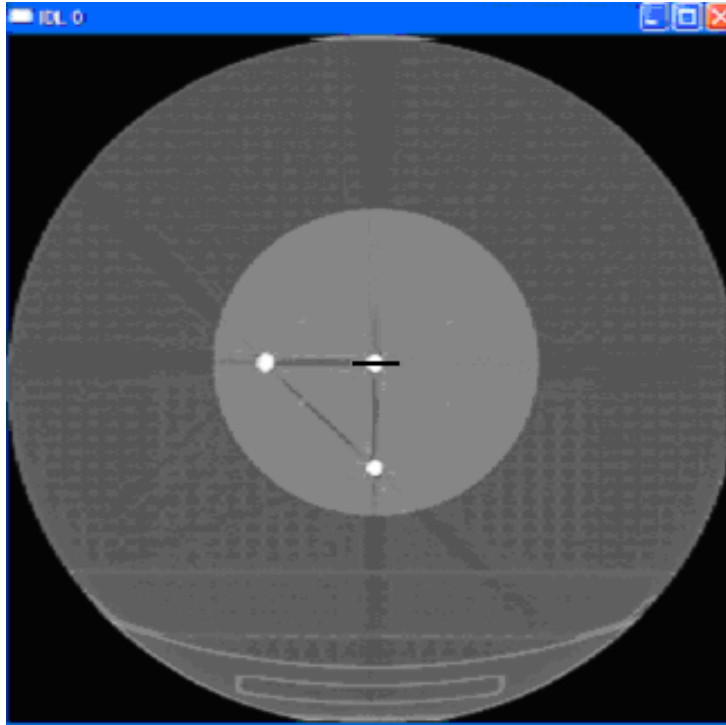


Figure 12: Screenshot showing the line for drawing a profile across the object on the CT image.

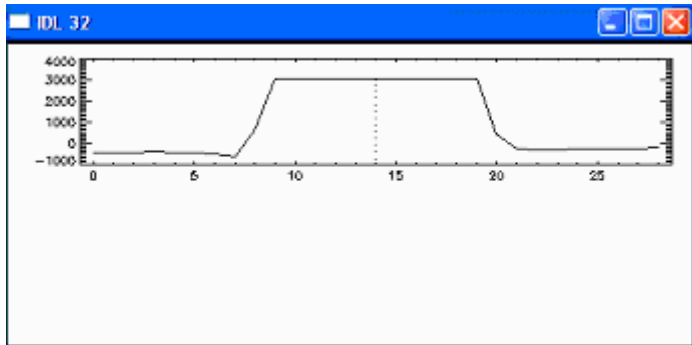


Figure 13: Screenshot displaying the profile of the selected object on the CT image.

#### **4.2.2.2 Maximum-Pixel Value Method**

For this method, a custom IDL procedure calculates the center co-ordinate of the object based on the pixel intensity values. In a CT or a PET image, the object is the pixels having maximum intensity value. The user specifies the approximate range of pixels within which the object is located. For determining the x coordinates of the object, the computer program checks from one end for the maximum values. Once the first maximum value is found, its coordinate is stored and the search begins again but from the other end. The program generates the average of these two coordinates, which is our required x coordinate for the source. This is repeated for the y coordinate with the program searching the maximum values in the y direction. In this way the location of the center of an object is obtained from the given range of values within which the object is situated. This method is illustrated in Figure 14 and Figure 15. Figure 14 shows the Maximum-Pixel Value method applied to the PET image of a the Triple-line Source phantom. The square region shown is the selected region of interest given as input to the main procedure in IDL. The computer program checks for the maximum pixel value from one end, P, and reaches the point A. This coordinate at A is stored and then the computer program checks for the maximum pixel value from the other end, Q, to locate the maximum pixel value (at A again) and this coordinate is also stored. The average of these coordinates is found and hence the center of the object of interest which is the coordinate of A. Figure 15 shows the Maximum-Pixel Value method applied to the CT image of Triple-line Source phantom. The region of interest is given as input with the starting coordinate as P and the computer program checks for the maximum pixel value. Once the maximum value is obtained, at A, the program stores this coordinate. Then the program

checks for the maximum pixel value from the other end, Q. The maximum value from the other end is found at B and the computer program stores the coordinates of B. Then the average of the coordinates A and B is calculated which is the required center coordinate of the object of interest.

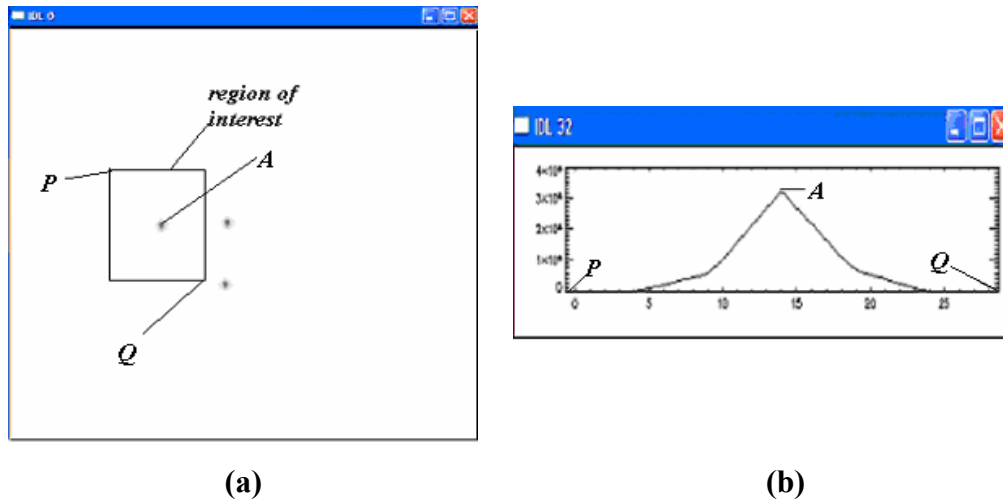


Figure 14: Illustration of the Maximum-Pixel Value method using (a) PET image of a Triple-line Source phantom and (b) the profile of the object in the PET image of the Triple-line Source phantom.

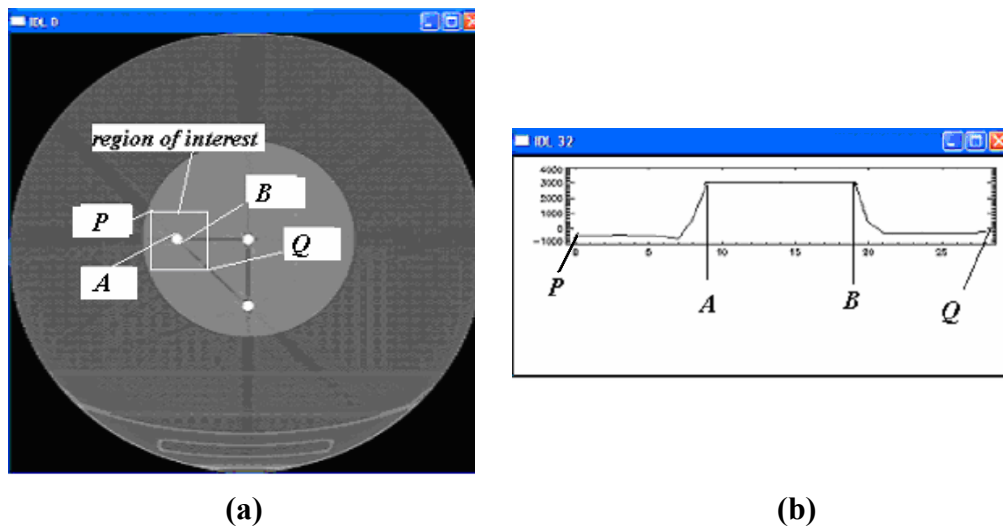


Figure 15: Illustration of the Maximum-Pixel Value method using (a) CT image of a Triple-line Source phantom and (b) the profile of the object in the CT image of the Triple-line Source phantom.

### 4.2.2.3 Curve-fitting Method

In this method an analytic function is fit to the source image. The PET images are fit to a Gaussian function; with sufficient counts, the image of a point object is Gaussian in shape. Initial estimates for the height, center and width (standard deviation) of the Gaussian curve are specified and the fit is obtained using IDL's least-squares curve-fitting algorithm. The fitted parameter values are obtained as a result. As with the Maximum-Pixel Value method, the user specifies the range of image coordinates that comprises the object. To determine the absolute coordinates of the center of the object in the PET image we add the fitted value of the center of the curve to the beginning coordinate of the range given as input.

For the CT images of the Triple-line Source phantom, the images of the sources are also fit to a Gaussian function; visual inspection showed that the small line sources look approximately Gaussian. However, the larger objects of the other phantoms cannot be approximated as Gaussian or even a simple analytic function. For the other phantoms, a square region is drawn with pixels of the same intensity as that of the objects of the phantom. The dimensions of this region are equivalent to the known diameter of the objects of the phantom. Similar to the Maximum-Pixel Value method, the user specifies the approximate range of pixels within which the object is located. To determine the coordinates of the object, a computer program sequentially maps the generated region from one of the ends specified by the user and determines the average difference between the pixel intensities of the image and the overlying square region. When the region superimposes over the object, the difference between the average pixel intensities reaches

a minimum. The center coordinates of the region at that particular location is taken as the desired center coordinate of the object of the phantom.

### **4.3 Determination of PET Resolution**

The Curve-fitting Method also estimates the spatial resolution of the PET scanner. Spatial resolution is determined from the fitted standard deviation of the Gaussian function. From the standard deviation ( $\sigma$ ) of the curve, the object size expressed as the full width at half maximum (FWHM) is given by Equation 2.

$$FWHM = 2.3548 * (\sigma) \quad (\text{Equation 2})$$

The estimated spatial resolution is then given by Equation 3 where  $S_o$  is the known object diameter.

$$\text{Resolution} = \sqrt{(FWHM)^2 - (S_o)^2} \quad (\text{Equation 3})$$

For this thesis, resolution is estimated for all the different phantoms using the Curve-fitting method and is checked for correlations with the measured alignment error results. One must note that this is only a rough approximation to the true spatial resolution. It is adequate for checking consistency between the PET images of the objects of different sizes, but cannot be interpreted as an accurate measurement of the spatial resolution of the PET scanner.

# CHAPTER 5

## RESULTS

### 5.1 CT Quality Assurance

This section describes the CT QA results obtained from the Gammex 464 phantom, both before and after modification. All tests for determining different CT parameters were performed only once using the Gammex phantoms.

#### 5.1.1 CT Number Calibration

CT number calibration is performed as per the instructions given in the Instruction Manual for the ACR CT Accreditation Phantom. The CT acquisition parameters are presented in Table 4. Figure 16 illustrates the features of the Gammex 464 phantom used for CT number calibration. To pass the CT number calibration test, the measured CT numbers must fall within specified ranges for each material in the phantom. The CT number ranges are given in the Instruction Manual and summarized in Table 5.

The CT number calibration test was performed using the Gammex phantom before modification and then repeated using the Gammex phantom after modification with both the acrylic insert and the solid water insert. The results are shown in Figure 17. The CT numbers of all materials using the original and modified phantoms are within the range of values as given in the Instruction Manual, except for the acrylic material in the unmodified Gammex phantom (Figure 17c).

Table 4: CT acquisition and display parameters to perform CT number calibration as given in the instruction manual using the Gammex phantom

<b>CT Acquisition Parameter</b>	<b>Value</b>
kVp Setting	120 kV
mA Setting	55 mA
Technique	Adult Abdomen Technique
Slice Thickness	3.75 mm
Window Width (WW)	400
Window Level (WL)	0
Location	S0*

\* The alignment lasers are aligned on the center of module 1 of the phantom. This position is marked as S0 and all other image slices are referenced as millimeters superior (S) or inferior (I) to this mark

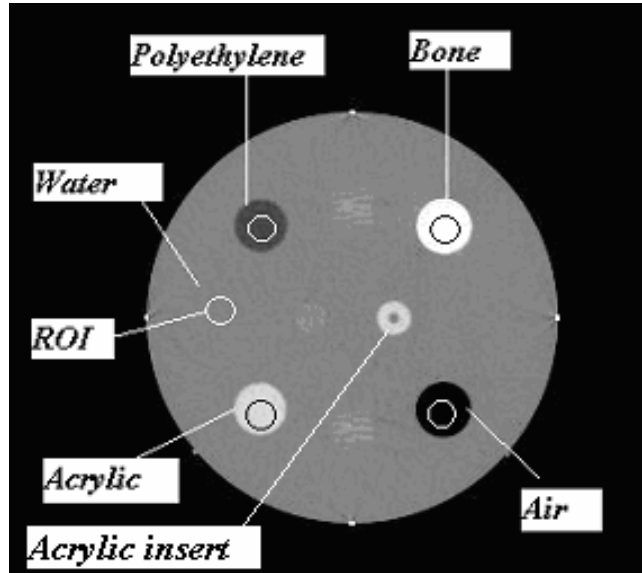


Figure 16: CT image of the modified Gammex phantom with acrylic insert displaying different materials of different densities used for CT number calibration.

Table 5: Acceptable CT number ranges for the Gammex phantom, specified by the ACR<sup>20</sup>

<b>Material</b>	<b>Minimum CT Number (HU)</b>	<b>Maximum CT Number (HU)</b>
Polyethylene	-107	-87
Bone	850	970
Acrylic	110	130
Air	-1005	-970
Water	-7	7

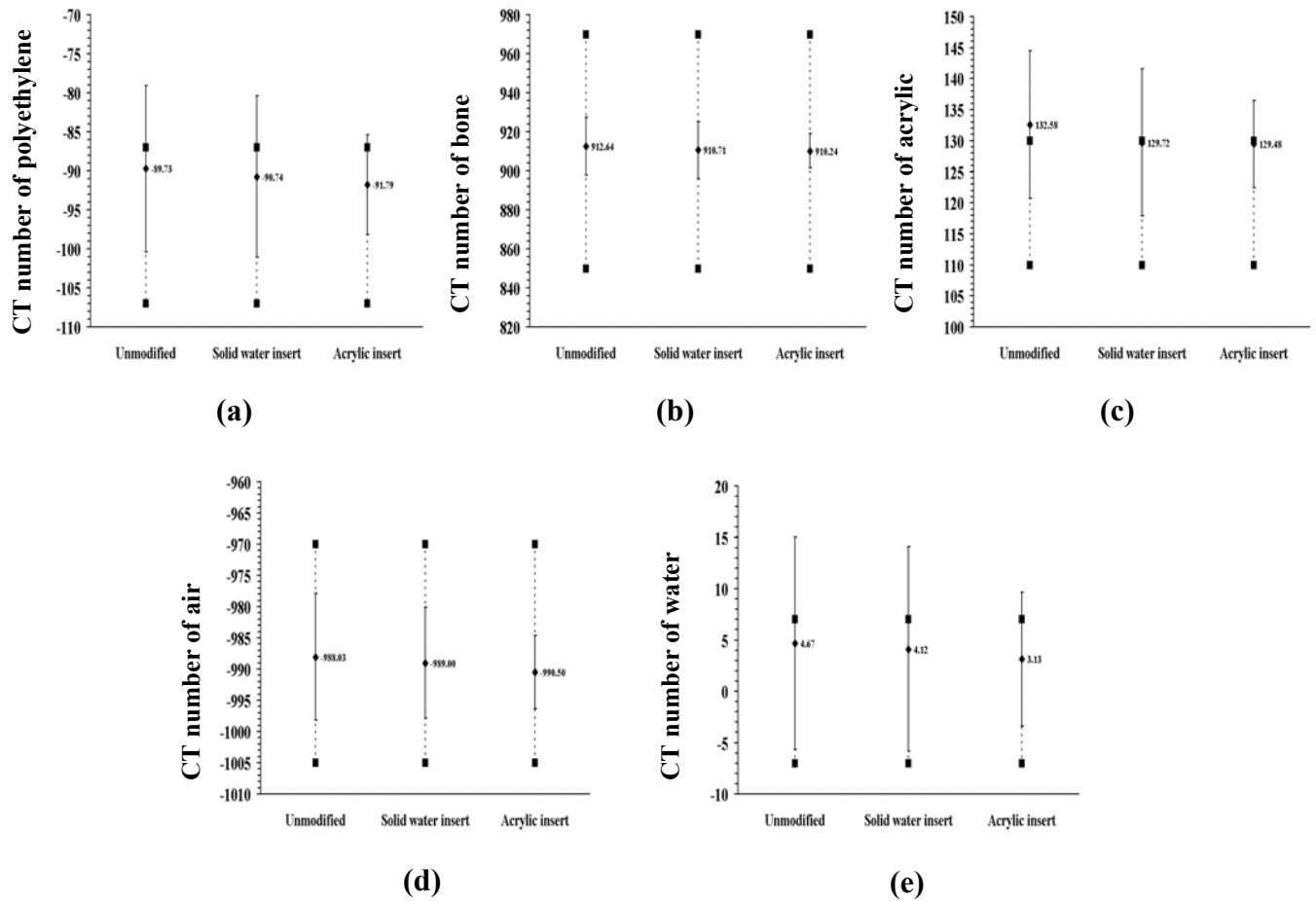


Figure 17: CT number calibration for the different materials of the unmodified Gammex phantom and the modified Gammex phantom with either solid water or acrylic insert. The materials are (a) polyethylene, (b) bone, (c) acrylic, (d) air and (e) water.

## 5.1.2 Slice Thickness

### 5.1.2.1 Determination of Slice Thickness at 120 kVp

CT acquisition parameters for determination of slice thickness were set according to instructions in the ACR Accreditation Manual, as summarized in Table 6. Figure 18 displays the slice thickness wires used for measurement of slice thickness. Shown in Figure 19, the slice thickness measured with the modified Gammex phantom with solid water or acrylic inserts equals the slice thickness specified in the acquisition set up. The

slice thickness measured with the unmodified Gammex phantom is marginally different from the acquisition specification. Given the semi-quantitative method used, we conclude that all three phantoms are showing essentially the same behavior.

### **5.1.2.2 Verification of CT Number vs. kVp**

The acquisition parameters are the same as those noted in Table 6 for the determination of slice thickness except that slice thickness is fixed at 3.75 mm and measurements are made at 80 kV, 100 kV, 120 kV, and 140 kV. The measured CT numbers were similar irrespective of the phantom used. While the CT number of water increases slightly with increase in kV, it is within the CT number ranges given in the Gammex manual (Figure 20).

### **5.1.3 Low Contrast Resolution**

CT acquisition parameters for determination of low contrast resolution were set according to instructions in the ACR Accreditation Manual, as summarized in Table 7. Low contrast resolution is measured using two different techniques, Routine Head technique and Adult Abdomen technique. The CT number of solid water on the largest low-contrast object as well as on the next object is found (Figure 21). Also the diameter of the smallest cylinder that is clearly visible is noted. The measured values using Routine Head technique are presented in Table 8 and using Adult Abdomen technique in Table 9. It can be observed that the measured values are consistent and within the range given in the Gammex manual.

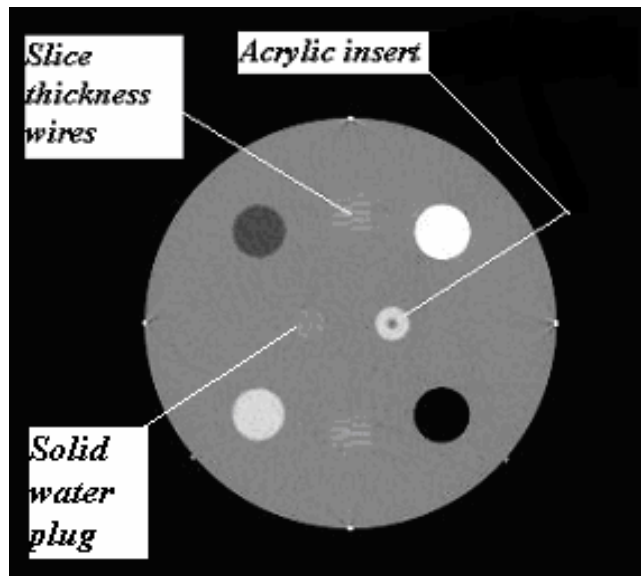


Figure 18: CT image of the modified Gammex phantom with acrylic insert showing the 0.5 mm wires used in determination of slice thickness.

Table 6: CT acquisition and display parameters to determine slice thickness using Gammex phantom

CT Acquisition Parameter	Value
kVp	120 kV
mA	40-50 mA
Technique	Adult Abdomen Technique
Slice Thickness	2.5 mm, 5 mm, 7.5 mm
Window Width (WW)	400
Window Level (WL)	0
Location	S0*

\*Relative to the center of Module 1.

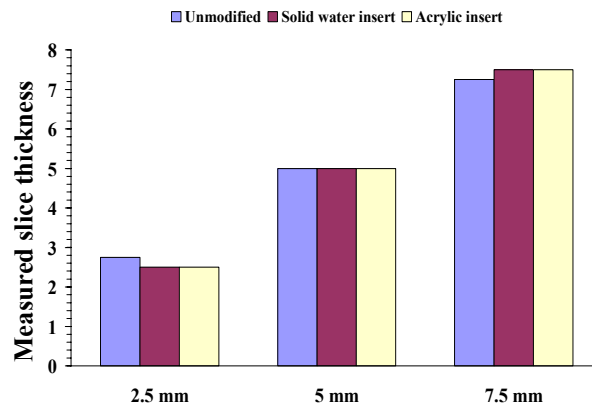


Figure 19: Slice thickness measured at constant 120 kVp setting. The specified acquisition slice thicknesses were 2.5 mm, 5 mm, and 7.5 mm.

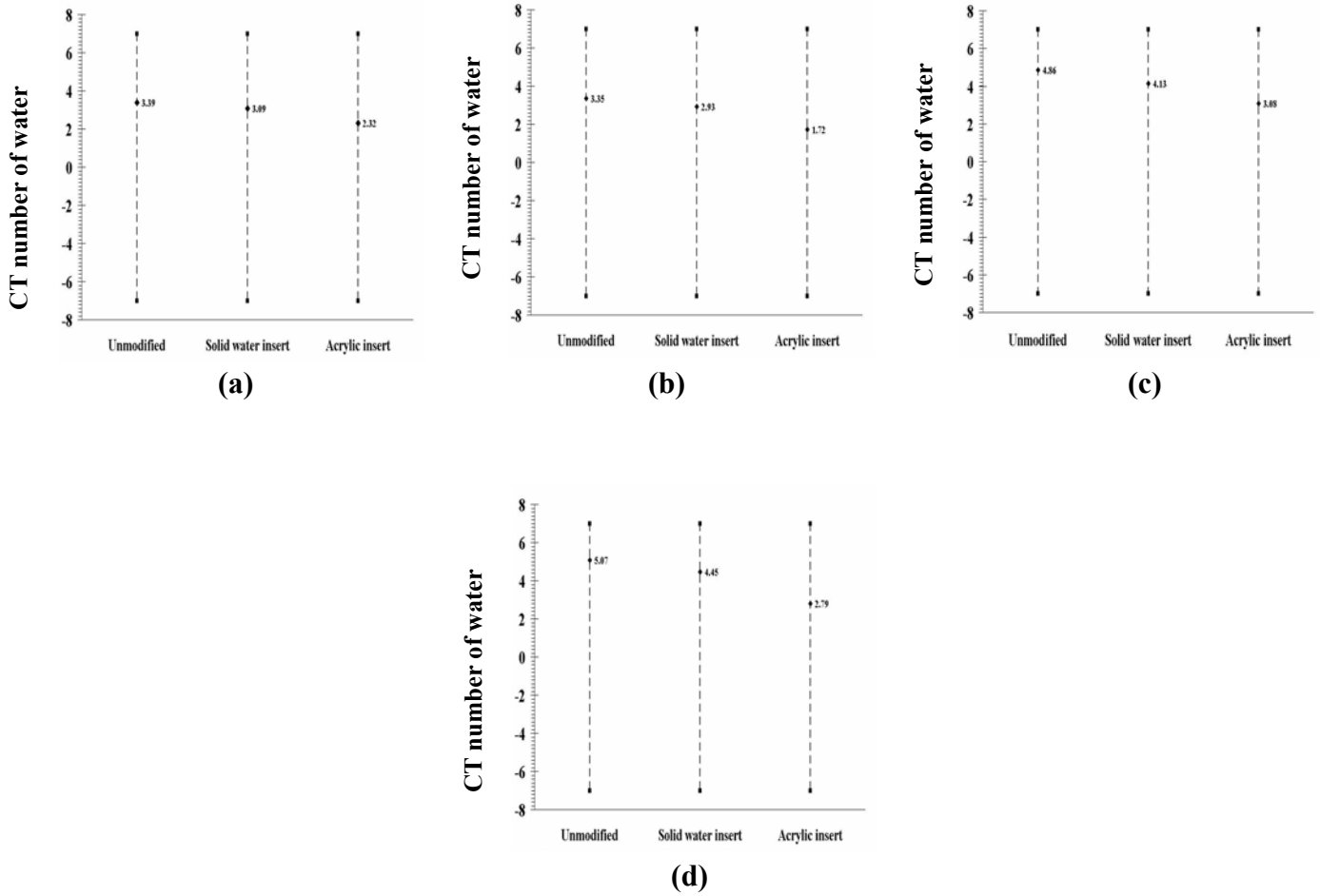


Figure 20: CT number of water measured for a constant slice thickness as a function of kVp setting for (a) 80 kVp, (b) 100 kVp, (c) 120 kVp, and (d) 140 kVp.

Table 7: CT acquisition and display parameters to determine low contrast resolution using Gammex phantom

CT Acquisition parameter	Value
kVp Setting	120 kV
mA Setting	(200-220) mA
Slice Thickness	3.75 mm
Window Width (WW)	100
Window Level (WL)	100
Location	S40*

\*Location is 40 mm superior to the center of Module 1

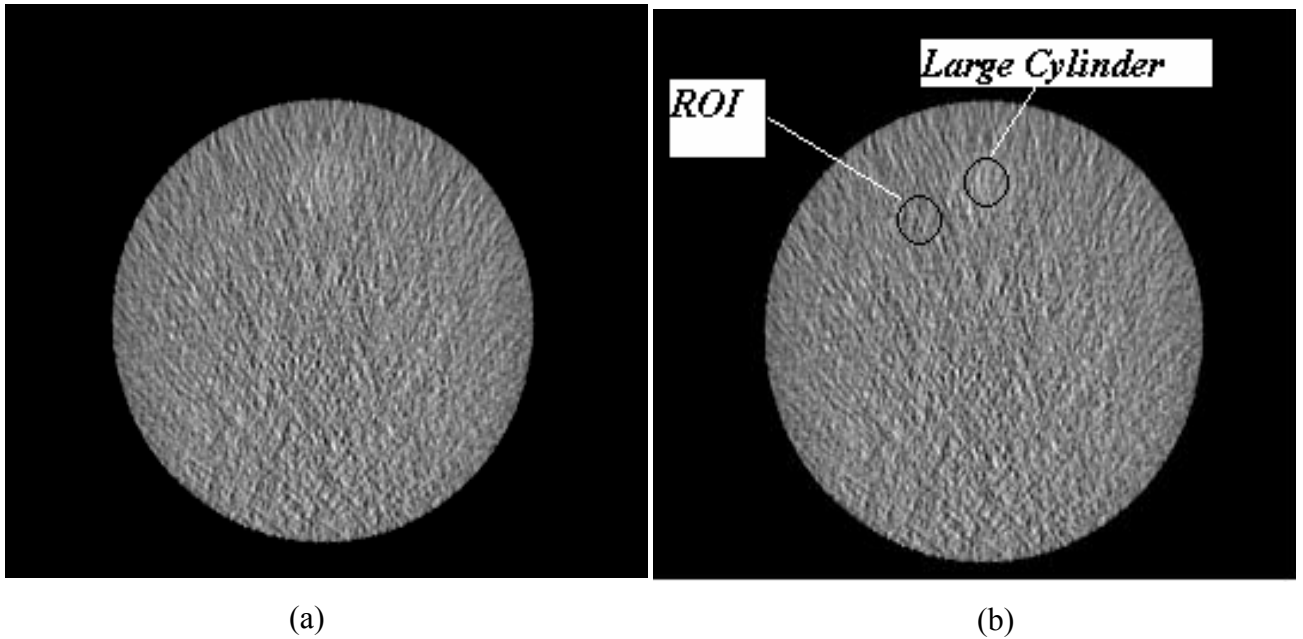


Figure 21: CT image at S40 location illustrating determination of low contrast resolution (a) without region of interests (ROI) shown and (b) with ROIs shown.

Table 8: Low contrast resolution performed using Routine Head technique with the Gammex phantoms

<b>Phantom</b>	<b>Diameters of visible cylinders (mm)</b>	<b>CT number (large cylinder) (HU)</b>	<b>CT number (next largest cylinder) (HU)</b>
Gammex 464	6	94.6	89.37
Modified Gammex (Acrylic)	6	99.12	92.51
Modified Gammex (Solid Water)	6	97.93	91.58

Table 9: Low contrast resolution performed using Adult Abdomen technique with the Gammex phantoms

<b>Phantom</b>	<b>Diameters of visible cylinders (mm)</b>	<b>CT number (large cylinder) (HU)</b>	<b>CT number (next largest cylinder) (HU)</b>
Gammex 464	6	95.54	89.05
Modified Gammex (Acrylic)	6	97.73	92.19
Modified Gammex (Solid Water)	6	98.31	90.74

### 5.1.4 High Contrast Resolution

CT acquisition parameters for measurement of high contrast resolution are summarized in Table 10. High contrast resolution, or highest spatial frequency, is determined with both Adult Abdomen technique and High Resolution Chest technique. Both techniques are performed at 120 kV. Table 11 shows that the measured highest spatial frequency is the same for all three phantoms used. Figure 22 displays CT images of the modified Gammex phantom with acrylic insert, showing the high resolution bars used for measuring the highest spatial frequency.

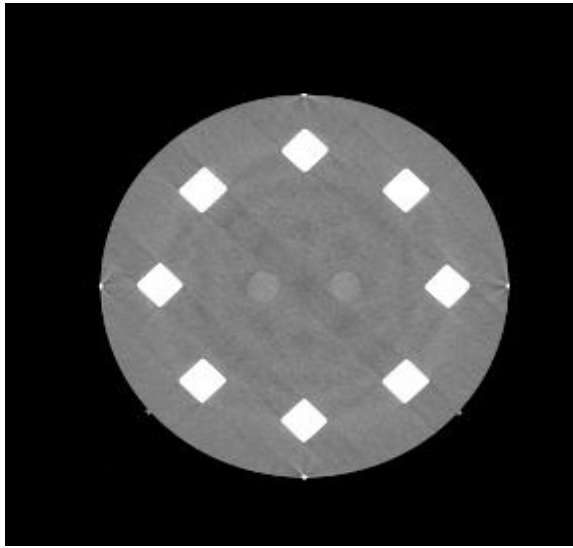
### 5.1.5 Uniformity

Table 12 gives the CT acquisition and display parameters for the determination of uniformity. CT number is measured at the 3, 6, 9 and 12 o'clock positions, in Module 3 of the Gammex phantom (Figure 23b), as well as at the center. These CT numbers at the periphery are subtracted from the CT number obtained at the centre. The average difference is reported as the uniformity. Figure 23(a) shows the uniformity results measured for the different versions of the Gammex phantom.

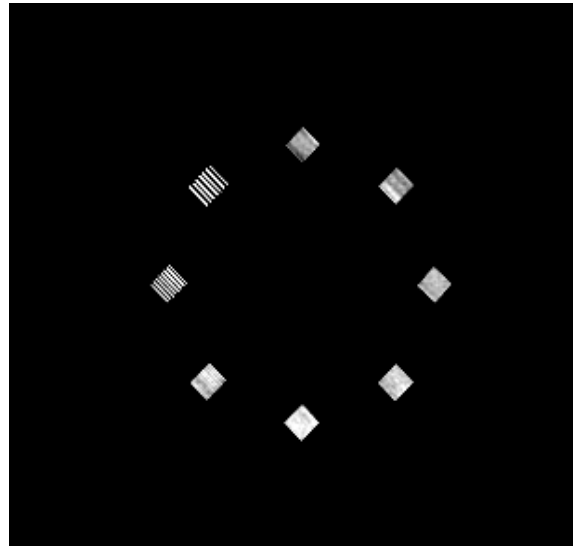
Table 10: CT acquisition parameters used to measure high contrast resolution

<b>CT Acquisition parameter</b>	<b>Value</b>
kVp Setting	120 kV
Slice Thickness	3.75 mm
Window Width (WW)	100
Window Level (WL)	1100
Location	S120*

\*Location is 120 mm superior to the center of Module 1.



(a)



(b)

Figure 22: CT image of Module 4 of the modified Gammex phantom with acrylic insert illustrating determination of high contrast resolution at (a) a soft tissue window level, and (b) the recommended window level.

Table 11: High contrast resolution measured using High Resolution Chest technique and Adult Abdomen technique

Phantom	mA Setting (mA)		Highest spatial frequency (lp/cm)	
	High Resolution Chest technique	Adult Abdomen technique	High Resolution Chest technique	Adult Abdomen technique
Unmodified Gammex	39	40	7	7
Acrylic insert	39	40	7	7
Solid Water insert	50	59	7	7

Table 12: CT acquisition and display parameters to determine the uniformity using the Gammex phantom

CT Acquisition parameter	Value
kVp Setting	120 kV
mA Setting	130 mA
Technique	Adult Abdomen Technique
Slice Thickness	3.75mm
Window Width (WW)	100
Window Level (WL)	0
Location	S80*

\* Location is 80 mm superior to the center of Module 1

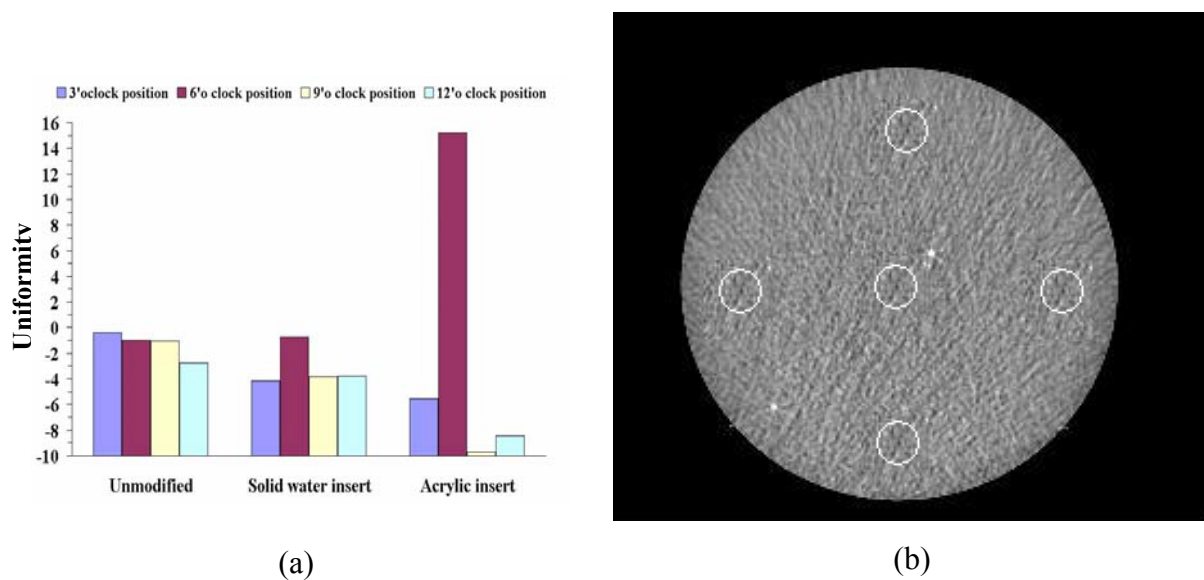


Figure 23: (a) Uniformity measured with the modified and unmodified Gammex phantom, and (b) CT image of the modified Gammex phantom with acrylic insert at location S80 illustrating placement of center and edge regions of interest (ROI) for uniformity measurement.

## 5.2 PET/CT Alignment Tests

This section presents the PET/CT alignment results. Each section presents the results for all of the phantoms, using one of the analysis methods described in Chapter 4.

### 5.2.1 Results from Manual Method

#### 5.2.1.1 Modified Gammex Phantom with Acrylic Insert

Figure 24 presents the PET/CT alignment test data obtained for the modified Gammex phantom with acrylic insert. The data represent the average measured x and y coordinates of the center of the acrylic insert source, for CT and the four different PET acquisitions. Table 13 reports the measured alignment errors for the four PET acquisitions relative to the CT data. Except for the y-coordinate error with the 3D PET acquisitions, the alignment error is on the order of 1 mm. For 3D PET, the y-coordinate error is substantially larger, nearly 3 mm. One also sees that for 2D and 3D PET, the y-coordinate error is larger than the x-coordinate error.

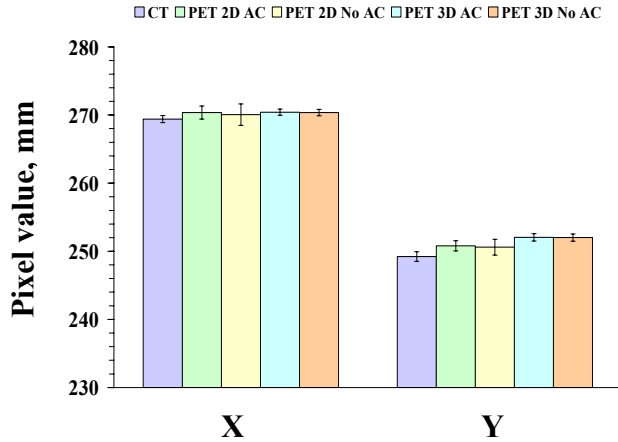


Figure 24: Measured center coordinates using the Manual method for the modified Gammex phantom with acrylic insert.

Table 13: Measured PET/CT alignment errors for the modified Gammex phantom with acrylic insert using the Manual method

Alignment error (mm)	2D		3D	
	Attenuation Correction	No Attenuation Correction	Attenuation Correction	No Attenuation Correction
$\Delta X \pm \sigma$	$0.95 \pm 0.28$	$0.65 \pm 0.42$	$1.00 \pm 0.20$	$0.95 \pm 0.20$
$\Delta Y \pm \sigma$	$1.57 \pm 0.28$	$1.37 \pm 0.37$	$2.81 \pm 0.26$	$2.79 \pm 0.25$

### 5.2.1.2 Modified Gammex Phantom with Solid Water Insert

The PET/CT alignment test data obtained using the Manual method for the modified Gammex phantom with solid water insert are illustrated in Figure 25. Table 14 summarizes the measured alignment errors between the CT and the four PET acquisitions. Although there was a difficulty for distinguishing the edge of the insert and the surrounding phantom material which is also solid water, the measured alignment errors with this phantom are less than the errors with the acrylic insert. Again, the y-coordinate error is larger than the x-coordinate error.

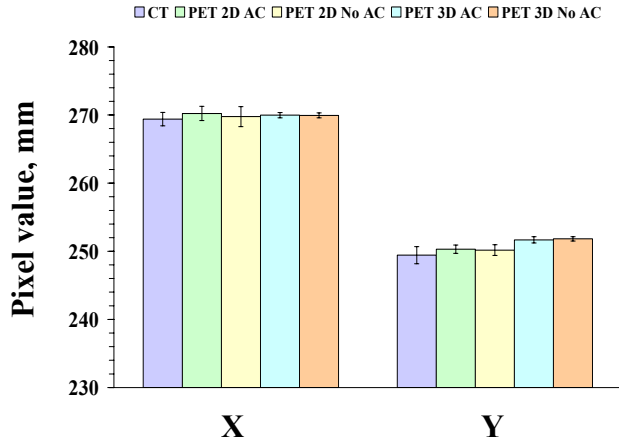


Figure 25: Measured center coordinates using the Manual method for the modified Gammex phantom with solid water insert.

Table 14: Measured PET/CT alignment errors for the modified Gammex phantom with solid water insert using the Manual method

Alignment error (mm)	2D		3D	
	Attenuation Correction	No Attenuation Correction	Attenuation Correction	Attenuation Correction
$\Delta X \pm \sigma$	$0.83 \pm 0.41$	$0.36 \pm 0.49$	$0.57 \pm 0.32$	$0.54 \pm 0.32$
$\Delta Y \pm \sigma$	$0.88 \pm 0.43$	$0.75 \pm 0.45$	$2.26 \pm 0.41$	$2.41 \pm 0.40$

### 5.2.1.3 Triple-line Source Phantom

Figure 26 presents the PET/CT alignment test data for the Triple-Line Source phantom using the Manual method. Table 15 summarizes the measured alignment errors for the different PET/CT acquisitions. The measured alignment errors were relatively consistent among the different PET acquisitions. The measured errors for the y-coordinates were larger than those for the x-coordinates for all three sources. Combining the x and y alignment errors for all the line sources, the average alignment error is on the order of 0.5 mm for all the acquisitions except for the 2D acquisition of the y-coordinate for which it is on the order of 1 mm.

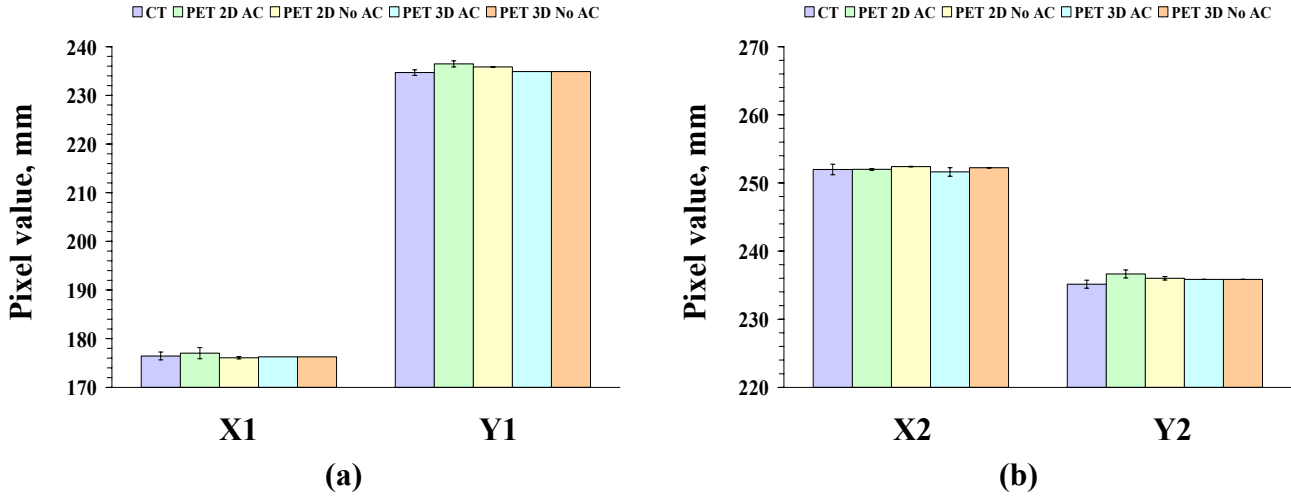


Figure 26: Measured center coordinates using the Manual method for the triple line source phantom without rotation for (a) first source and (b) second source.

Table 15: Measured PET/CT alignment errors for the triple line source phantom using the Manual method

Sources	Alignment error (mm)	2D		3D	
		Attenuation Correction	No Attenuation Correction	Attenuation Correction	No Attenuation Correction
Source 1	$\Delta X1 \pm \sigma$	$0.59 \pm 0.37$	$0.37 \pm 0.26$	$0.17 \pm 0.26$	$0.17 \pm 0.26$
	$\Delta Y1 \pm \sigma$	$1.79 \pm 0.24$	$1.17 \pm 0.18$	$0.19 \pm 0.18$	$0.19 \pm 0.18$
Source 2	$\Delta X2 \pm \sigma$	$0.01 \pm 0.25$	$0.42 \pm 0.24$	$0.37 \pm 0.28$	$0.25 \pm 0.24$
	$\Delta Y2 \pm \sigma$	$1.49 \pm 0.23$	$0.86 \pm 0.20$	$0.70 \pm 0.19$	$0.70 \pm 0.19$
Source 3	$\Delta X3 \pm \sigma$	NA	NA	NA	NA
	$\Delta Y3 \pm \sigma$	NA	NA	NA	NA
Average	$\Delta \bar{X} \pm \sigma$	$0.30 \pm 0.22$	$0.40 \pm 0.18$	$0.27 \pm 0.19$	$0.21 \pm 0.18$
	$\Delta \bar{Y} \pm \sigma$	$1.64 \pm 0.17$	$1.01 \pm 0.13$	$0.45 \pm 0.13$	$0.45 \pm 0.13$

NA: not available because of the air bubble in the third insert of the Triple-Line Source phantom while acquiring the PET images

### 5.2.1.4 Triple-line Source Phantom Rotated by 45°

Figure 27 illustrates center coordinate measurements using the Manual method for the sources of the Triple-Line Source phantom rotated by 45°. Table 16 reports the measured alignment errors for the four PET acquisitions relative to the CT data. The measured alignment errors for the four PET acquisitions relative to the CT data. The measured y-coordinate errors are larger than the x-coordinate errors. Also the measured alignment errors were considerably larger than the errors for the triple-line source phantom without any rotation.

Table 16: Measured PET/CT alignment errors for the triple line source phantom rotated by 45° using the Manual method

Sources	Alignment error (mm)	2D		3D	
		Attenuation Correction	No Attenuation Correction	Attenuation Correction	No Attenuation Correction
Source 1	$\Delta X1 \pm \sigma$	$0.65 \pm 0.07$	$0.65 \pm 0.07$	$0.42 \pm 0.22$	$0.65 \pm 0.07$
	$\Delta Y1 \pm \sigma$	$1.89 \pm 0.14$	$1.71 \pm 0.01$	$2.75 \pm 0.13$	$2.69 \pm 0.01$
Source 2	$\Delta X2 \pm \sigma$	$0.24 \pm 0.25$	$0.99 \pm 0.25$	$2.93 \pm 0.25$	$0.68 \pm 0.25$
	$\Delta Y2 \pm \sigma$	$1.07 \pm 0.10$	$1.52 \pm 0.14$	$2.33 \pm 0.15$	$2.73 \pm 0.09$
Source 3	$\Delta X3 \pm \sigma$	NA	NA	NA	NA
	$\Delta Y3 \pm \sigma$	NA	NA	NA	NA
Average	$\Delta \bar{X} \pm \sigma$	$0.45 \pm 0.13$	$0.83 \pm 0.13$	$1.68 \pm 0.17$	$0.67 \pm 0.13$
	$\Delta \bar{Y} \pm \sigma$	$1.48 \pm 0.09$	$1.61 \pm 0.07$	$2.54 \pm 0.10$	$2.71 \pm 0.05$

NA: not available because of the air bubble in the third insert of the Triple-Line Source phantom while acquiring the PET images

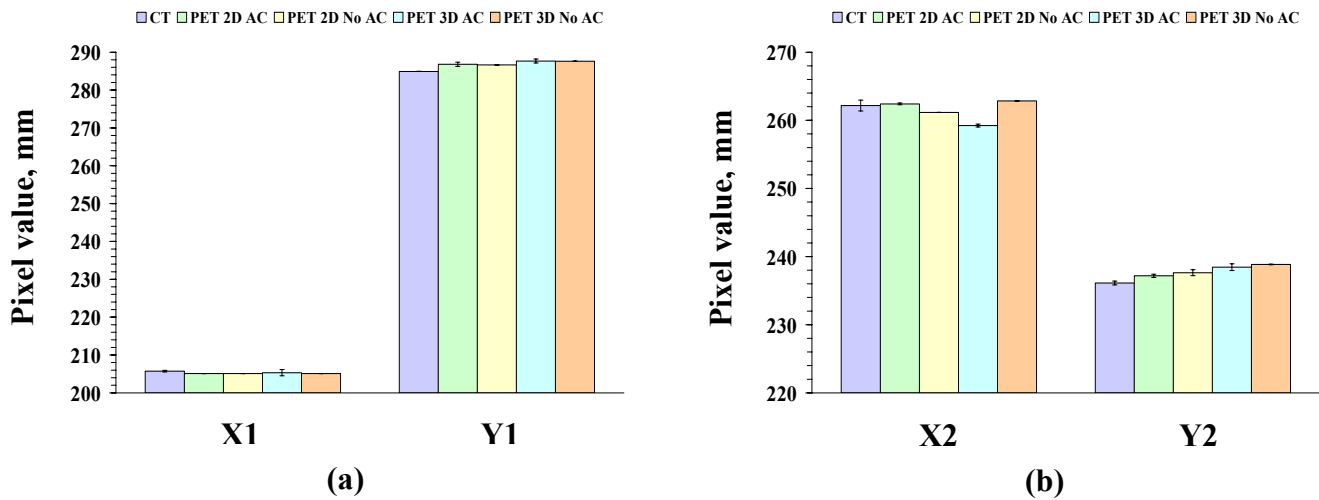


Figure 27: Measured center coordinates using the Manual method for the triple line source phantom rotated by 45° for (a) first source and (b) second source.

### 5.2.1.5 Hot Sphere Phantom

Figure 28 shows PET/CT alignment test results obtained using the Manual method for the Hot Sphere phantom. Table 17 provides the measured alignment errors for the different PET/CT acquisitions. Similar to most of the other phantoms, the y-coordinate error is larger than the x-coordinate error for this phantom using this method. The sphere with the smallest diameter gave the least error and as the diameter of the spheres increases, the measured alignment error also increases. Combining the x and y coordinates for all the sources of the phantom, the average alignment error for the x-coordinate for all the acquisitions is on the order of 1.5 mm while it is on the order of 2.5 mm for the y-coordinate.

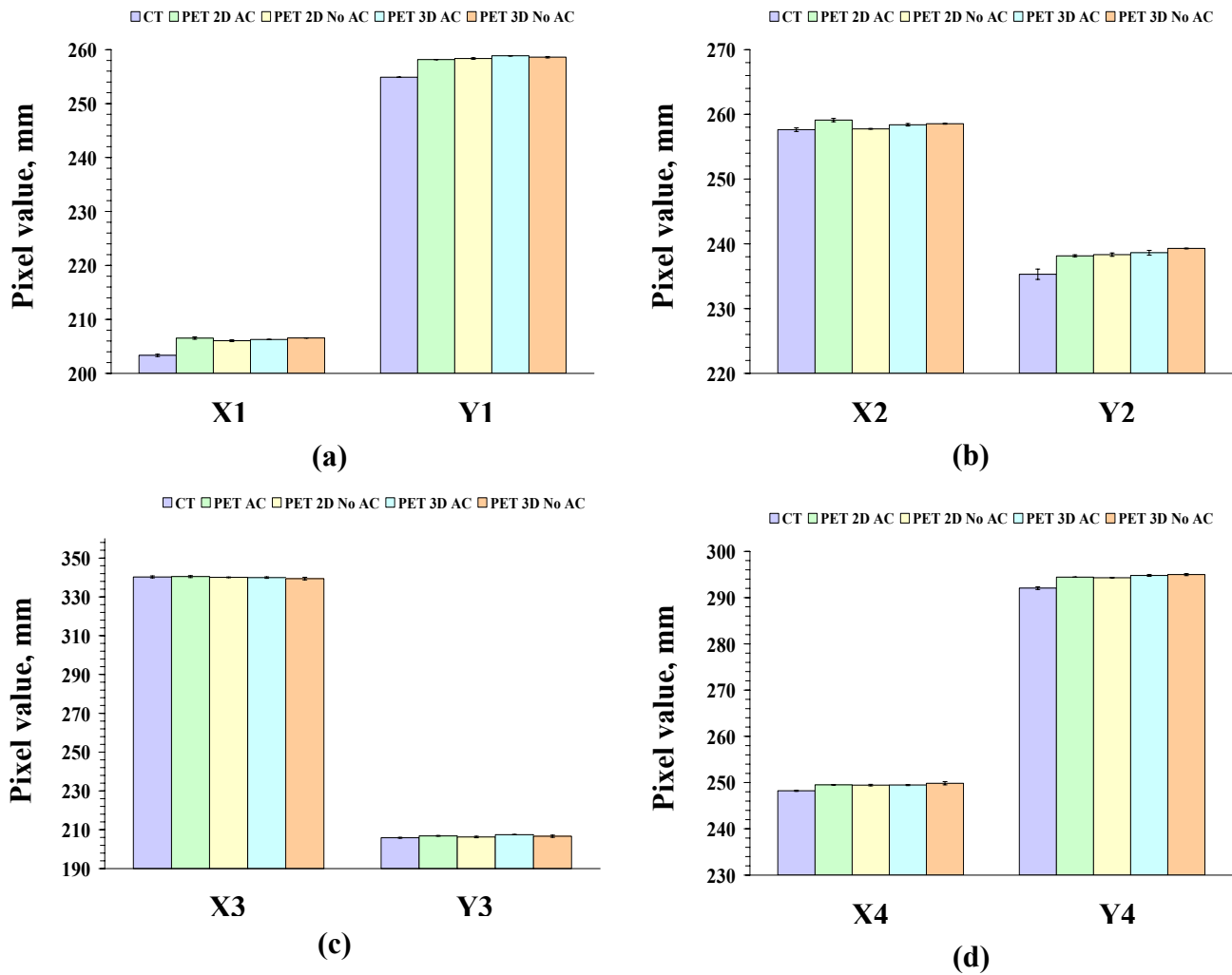


Figure 28: Measured center coordinates using the Manual method for the hot sphere phantom for (a) 18 mm diameter sphere, (b) 12 mm diameter sphere, (c) 6 mm diameter sphere, and (d) 8 mm diameter sphere.

Table 17: Measured PET/CT alignment errors for the hot sphere phantom using the Manual method

Diameter of sphere (mm)	Alignment error (mm)	2D		3D	
		Attenuation Correction	No Attenuation Correction	Attenuation Correction	No Attenuation Correction
18	$\Delta X1 \pm \sigma$	$3.20 \pm 0.07$	$2.71 \pm 0.08$	$2.94 \pm 0.07$	$3.22 \pm 0.07$
	$\Delta Y1 \pm \sigma$	$3.27 \pm 0.04$	$3.47 \pm 0.12$	$3.96 \pm 0.01$	$3.71 \pm 0.03$
12	$\Delta X2 \pm \sigma$	$1.47 \pm 0.11$	$0.12 \pm 0.09$	$0.75 \pm 0.10$	$0.91 \pm 0.09$
	$\Delta Y2 \pm \sigma$	$2.85 \pm 0.25$	$3.03 \pm 0.26$	$3.33 \pm 0.27$	$3.99 \pm 0.25$
6	$\Delta X3 \pm \sigma$	$0.16 \pm 0.21$	$0.22 \pm 0.17$	$0.38 \pm 0.19$	$0.88 \pm 0.23$
	$\Delta Y3 \pm \sigma$	$0.98 \pm 0.08$	$0.38 \pm 0.11$	$1.57 \pm 0.07$	$0.77 \pm 0.16$
8	$\Delta X4 \pm \sigma$	$1.30 \pm 0.04$	$1.23 \pm 0.06$	$1.25 \pm 0.05$	$1.63 \pm 0.10$
	$\Delta Y4 \pm \sigma$	$2.40 \pm 0.09$	$2.27 \pm 0.09$	$2.74 \pm 0.10$	$2.93 \pm 0.10$
Average	$\Delta \bar{X} \pm \sigma$	$1.53 \pm 0.06$	$0.96 \pm 0.05$	$1.14 \pm 0.06$	$1.22 \pm 0.07$
	$\Delta \bar{Y} \pm \sigma$	$2.38 \pm 0.07$	$2.29 \pm 0.08$	$2.90 \pm 0.07$	$2.85 \pm 0.08$

## 5.2.2 Results from Maximum-Pixel Value Method

### 5.2.2.1 Modified Gammex Phantom with Acrylic Insert

Figure 29 presents the PET/CT alignment test data obtained for the modified Gammex phantom with acrylic insert, using the Maximum-Pixel Value method. Table 18 records the measured alignment errors for the different PET acquisitions relative to the CT data. While the y-coordinate errors for the 3D acquisitions were again larger than that for the x-coordinate, the 2D acquisitions showed larger error for the x-coordinate than for the y-coordinate. For this method, the x-coordinate errors for all the PET/CT acquisitions were worse than those for the Manual method, but the y-coordinate errors for the 3D acquisitions for both the x and y coordinates are comparable for the two methods.

### 5.2.2.2 Modified Gammex Phantom with Solid Water Insert

Figure 30 presents the measured center coordinates of the object obtained using the Maximum-Pixel Value method for the modified Gammex phantom with the solid water insert. The measured alignment errors for the different acquisitions are summarized in Table 19. The uncertainties in the measured errors are larger than those found for this phantom using the Manual method.

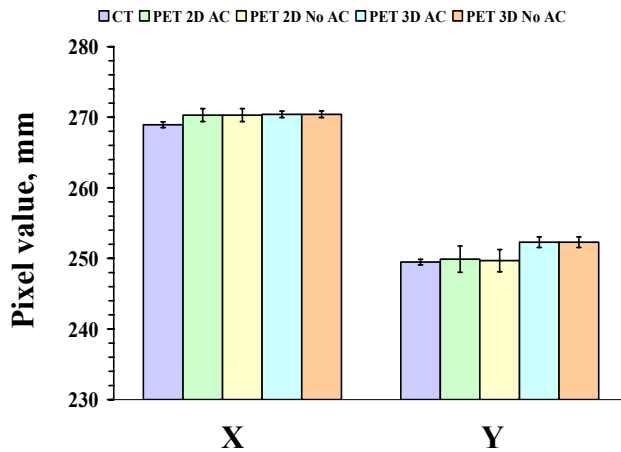


Figure 29: Measured center coordinates using the Maximum-Pixel Value method for the modified Gammex phantom with acrylic insert.

Table 18: Measured PET/CT alignment errors for the modified Gammex phantom with acrylic insert using the Maximum-pixel value method

Alignment error (mm)	2D		3D	
	Attenuation Correction	No Attenuation Correction	Attenuation Correction	No Attenuation Correction
$\Delta X \pm \sigma$	$1.37 \pm 0.25$	$1.37 \pm 0.25$	$1.47 \pm 0.16$	$1.48 \pm 0.16$
$\Delta Y \pm \sigma$	$0.42 \pm 0.45$	$0.20 \pm 0.39$	$2.81 \pm 0.21$	$2.81 \pm 0.21$

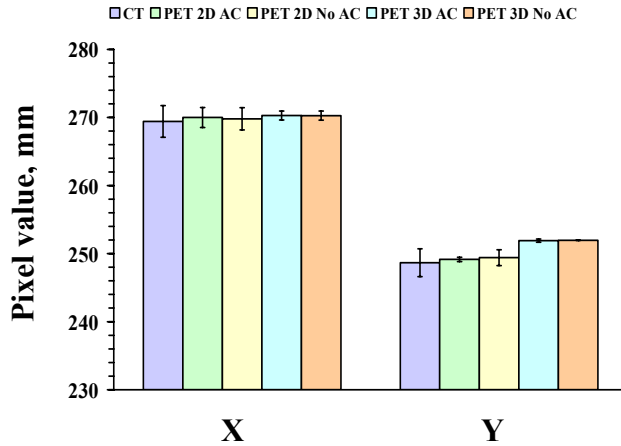


Figure 30: Measured center coordinates using the Maximum-Pixel Value method for the modified Gammex phantom with solid water insert.

Table 19: Measured PET/CT alignment errors for the modified Gammex phantom with solid water insert using the Maximum-pixel value method

Alignment error (mm)	2D		3D	
	Attenuation Correction	No Attenuation Correction	Attenuation Correction	No Attenuation Correction
$\Delta X \pm \sigma$	$0.58 \pm 0.76$	$0.39 \pm 0.77$	$0.87 \pm 0.69$	$0.85 \pm 0.69$
$\Delta Y \pm \sigma$	$0.48 \pm 0.59$	$0.74 \pm 0.65$	$3.24 \pm 0.59$	$3.29 \pm 0.59$

### 5.2.2.3 Triple-line Source Phantom

Figure 31 shows the center coordinates data for the three line sources of the Triple-Line Source phantom using the Maximum-Pixel Value method. Table 20 reports the measured alignment errors for the different PET acquisitions relative to the CT data. Again, 3D acquisitions generally show larger alignment errors than the 2D acquisitions. Both the x and y coordinate errors measured for the 3D acquisitions using this method are substantially larger than those using the Manual method. The error in the x coordinates is smaller compared to the errors in the y coordinates.

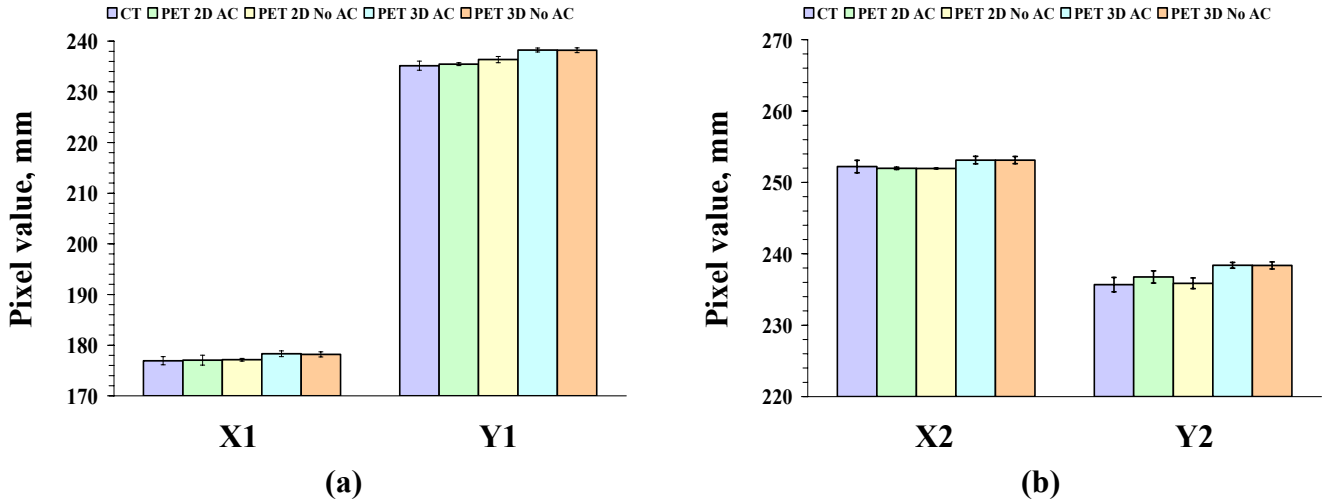


Figure 31: Measured center coordinates using the Maximum-Pixel Value method for the triple line source phantom without rotation for (a) first source and (b) second source.

Table 20: Measured PET/CT alignment errors for the triple line source phantom using the Maximum-pixel value method

Sources	Alignment error (mm)	2D		3D	
		Attenuation Correction	No Attenuation Correction	Attenuation Correction	No Attenuation Correction
Source 1	$\Delta X1 \pm \sigma$	$0.12 \pm 0.24$	$0.2 \pm 0.15$	$1.38 \pm 0.17$	$1.26 \pm 0.17$
	$\Delta Y1 \pm \sigma$	$0.31 \pm 0.17$	$1.21 \pm 0.19$	$3.09 \pm 0.18$	$3.06 \pm 0.18$
Source 2	$\Delta X2 \pm \sigma$	$0.24 \pm 0.16$	$0.26 \pm 0.16$	$0.91 \pm 0.18$	$0.91 \pm 0.18$
	$\Delta Y2 \pm \sigma$	$1.07 \pm 0.24$	$0.19 \pm 0.24$	$2.72 \pm 0.20$	$2.70 \pm 0.20$
Source 3	$\Delta X3 \pm \sigma$	NA	NA	NA	NA
	$\Delta Y3 \pm \sigma$	NA	NA	NA	NA
Average	$\Delta \bar{X} \pm \sigma$	$0.18 \pm 0.15$	$0.23 \pm 0.11$	$1.15 \pm 0.13$	$1.08 \pm 0.12$
	$\Delta \bar{Y} \pm \sigma$	$0.69 \pm 0.15$	$0.70 \pm 0.15$	$2.91 \pm 0.13$	$2.88 \pm 0.14$

NA: not available because of the air bubble in the third insert of the Triple-Line Source phantom while acquiring the PET images.

### 5.2.2.4 Triple-Line Source Phantom Rotated by 45°

Figure 32 gives the PET/CT alignment test data obtained for the Triple-Line Source phantom rotated by 45°. Table 21 provides the measured alignment errors for different PET/CT acquisitions. Combining the alignment errors in x and y coordinates for all the line sources, the average alignment error for all the acquisitions is on the order of 1 mm except for the y-coordinates with 3D acquisitions, for which it is on the order of 2.5 mm.

Table 21: Measured PET/CT alignment errors for the triple line source phantom rotated by 45° using the Maximum-pixel value method

Sources	Alignment error (mm)	2D		3D	
		Attenuation Correction	No Attenuation Correction	Attenuation Correction	No Attenuation Correction
Source 1	$\Delta X1 \pm \sigma$	$0.13 \pm 0.16$	$0.26 \pm 0.15$	$0.06 \pm 0.16$	$0.27 \pm 0.15$
	$\Delta Y1 \pm \sigma$	$1.43 \pm 0.06$	$1.43 \pm 0.06$	$2.59 \pm 0.12$	$2.93 \pm 0.29$
Source 2	$\Delta X2 \pm \sigma$	$0.69 \pm 0.17$	$0.47 \pm 0.21$	$3.05 \pm 0.50$	$0.75 \pm 0.23$
	$\Delta Y2 \pm \sigma$	$0.73 \pm 0.26$	$1.73 \pm 0.12$	$2.32 \pm 0.22$	$3.05 \pm 0.26$
Source 3	$\Delta X3 \pm \sigma$	NA	NA	NA	NA
	$\Delta Y3 \pm \sigma$	NA	NA	NA	NA
Average	$\Delta \bar{X} \pm \sigma$	$0.41 \pm 0.12$	$0.36 \pm 0.13$	$1.55 \pm 0.22$	$0.51 \pm 0.14$
	$\Delta \bar{Y} \pm \sigma$	$1.08 \pm 0.13$	$1.58 \pm 0.07$	$2.46 \pm 0.12$	$2.99 \pm 0.20$

NA: not available because of the air bubble in the third insert of the Triple-Line Source phantom while acquiring the PET images

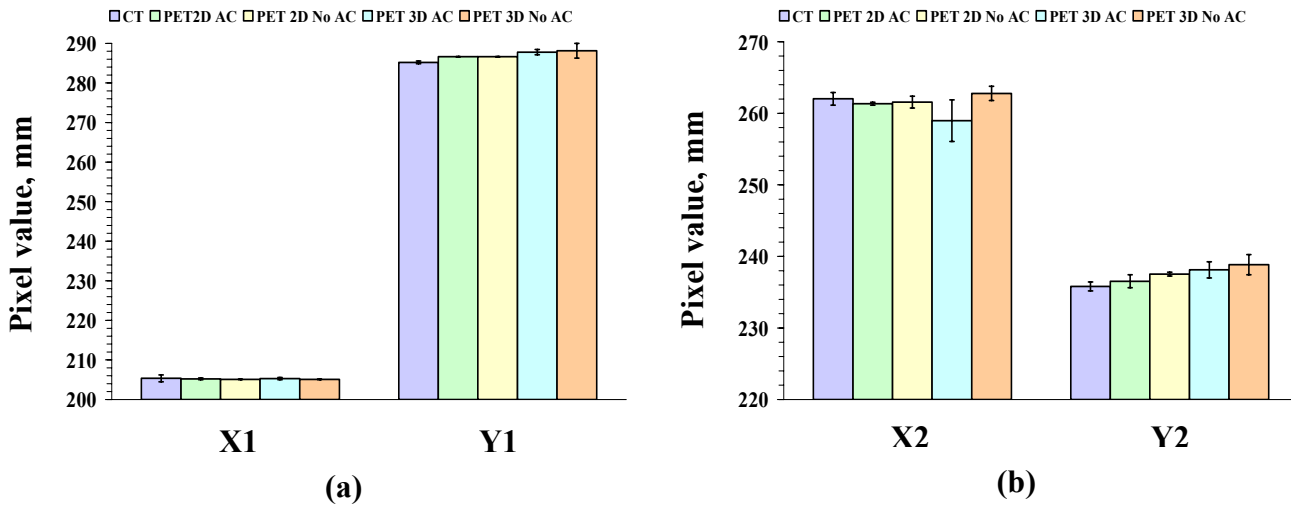


Figure 32: Measured center coordinates using the Maximum-Pixel Value method for the triple line source phantom rotated by 45° for (a) first source and (b) second source.

### 5.2.2.5 Hot Sphere Phantom

The PET/CT alignment test data obtained using the Maximum-Pixel Value method for the Hot Sphere phantom is illustrated in Figure 33. Table 22 summarizes the measured alignment errors between the CT and the four PET acquisitions. Similar to the alignment errors using the Manual method for this phantom, the measured errors increased with an increase in the diameter of the sources and the y-coordinate errors are larger than the x-coordinate errors. The measured alignment errors using this method for this phantom are comparable to that of the other phantoms.

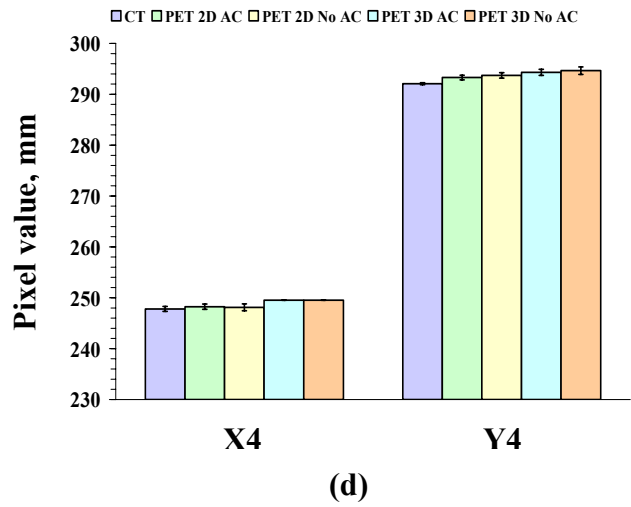
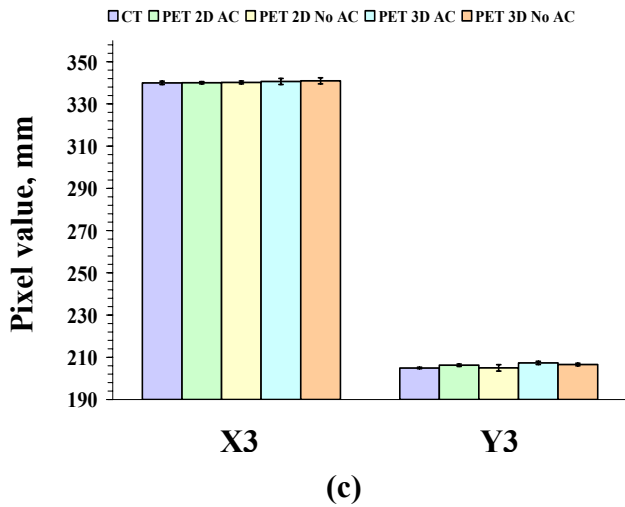
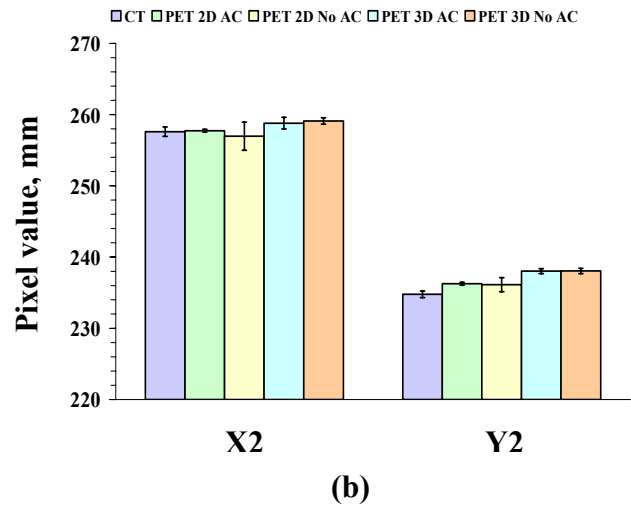
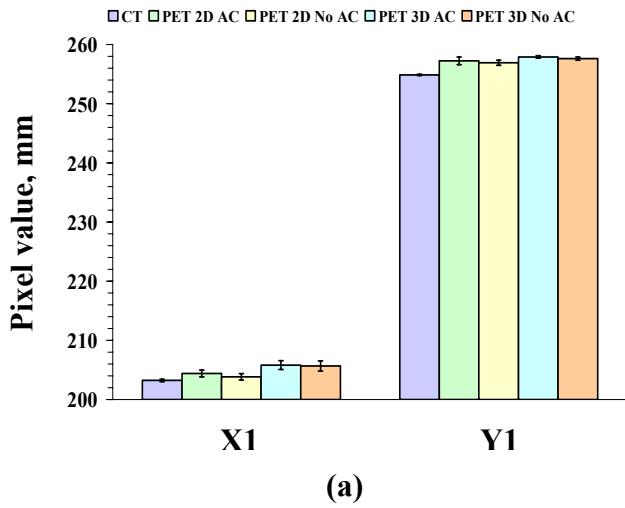


Figure 33: Measured center coordinates using the Maximum-Pixel Value method for the hot sphere phantom for (a) 18 mm diameter sphere, (b) 12 mm diameter sphere, (c) 6 mm diameter sphere, and (d) 8 mm diameter sphere.

Table 22: Measured PET/CT alignment errors for the hot sphere phantom using the Maximum-pixel value method

Diameter of sphere (mm)	Alignment error (mm)	2D		3D	
		Attenuation Correction	No Attenuation Correction	Attenuation Correction	No Attenuation Correction
18 mm	$\Delta X1 \pm \sigma$	$1.17 \pm 0.25$	$0.6 \pm 0.21$	$2.59 \pm 0.30$	$2.44 \pm 0.39$
	$\Delta Y1 \pm \sigma$	$2.37 \pm 0.29$	$2.05 \pm 0.17$	$3.03 \pm 0.08$	$2.76 \pm 0.12$
12 mm	$\Delta X2 \pm \sigma$	$0.13 \pm 0.15$	$0.63 \pm 0.61$	$1.19 \pm 0.30$	$1.49 \pm 0.20$
	$\Delta Y2 \pm \sigma$	$1.49 \pm 0.12$	$1.35 \pm 0.31$	$3.25 \pm 0.15$	$3.28 \pm 0.16$
6 mm	$\Delta X3 \pm \sigma$	$0.06 \pm 0.29$	$0.22 \pm 0.29$	$0.68 \pm 0.60$	$0.94 \pm 0.66$
	$\Delta Y3 \pm \sigma$	$1.33 \pm 0.26$	$0.08 \pm 0.57$	$2.43 \pm 0.31$	$1.62 \pm 0.27$
8 mm	$\Delta X4 \pm \sigma$	$0.44 \pm 0.21$	$0.31 \pm 0.23$	$1.72 \pm 0.09$	$1.72 \pm 0.09$
	$\Delta Y4 \pm \sigma$	$1.21 \pm 0.16$	$1.63 \pm 0.17$	$2.23 \pm 0.23$	$2.56 \pm 0.28$
Average	$\Delta \bar{X} \pm \sigma$	$0.45 \pm 0.31$	$0.44 \pm 0.23$	$1.55 \pm 0.67$	$1.65 \pm 0.63$
	$\Delta \bar{Y} \pm \sigma$	$1.60 \pm 0.60$	$1.28 \pm 0.54$	$2.74 \pm 0.76$	$2.56 \pm 0.70$

## 5.2.3 Results from Curve-fitting Method

### 5.2.3.1 Modified Gammex Phantom with Acrylic Insert

Figure 34 presents the PET/CT alignment test data for the modified Gammex phantom with acrylic insert using the Curve-fitting method. Table 23 records the measured alignment errors for the different PET acquisitions relative to the CT data. Similar to the other two methods, y-coordinate errors for 3D acquisitions were larger than that of the x-coordinate errors. The alignment errors measured using the Curve-fitting method show similar variation as those measured with the other methods.

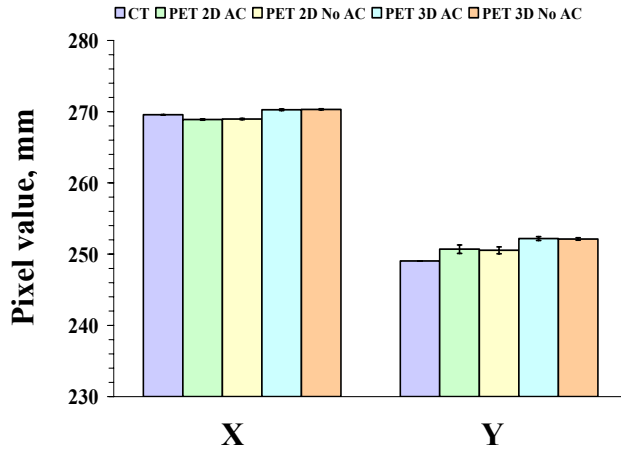


Figure 34: Measured center coordinates using the Curve-fitting method for the modified Gammex phantom with acrylic insert.

Table 23: Measured PET/CT alignment errors for the modified Gammex phantom with acrylic insert using the Curve-fitting method

Alignment error (mm)	2D		3D	
	Attenuation Correction	No Attenuation Correction	Attenuation Correction	No Attenuation Correction
$\Delta X \pm \sigma$	$0.66 \pm 0.02$	$0.60 \pm 0.02$	$0.71 \pm 0.03$	$0.76 \pm 0.02$
$\Delta Y \pm \sigma$	$1.67 \pm 0.15$	$1.51 \pm 0.12$	$3.16 \pm 0.07$	$3.10 \pm 0.04$

### 5.2.3.2 Modified Gammex Phantom with Solid Water Insert

Figure 35 illustrates the PET/CT alignment test data for the modified Gammex phantom with the solid water insert using the Curve-fitting method. The alignment errors measured for different PET/CT acquisitions are summarized in Table 24. Using this method, the measured errors are worse to those obtained with the modified Gammex phantom using the acrylic insert.

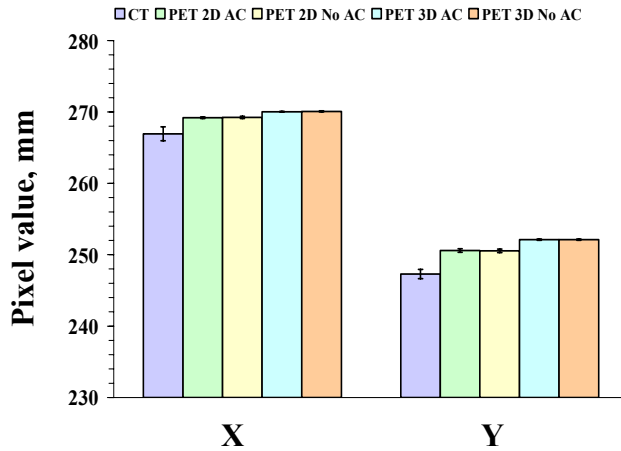


Figure 35: Measured center coordinates using the Curve-fitting method for the modified Gammex phantom with solid water insert.

Table 24: Measured PET/CT alignment errors values for the modified Gammex phantom with solid water insert using the Curve-fitting method

Alignment error (mm)	2D		3D	
	Attenuation Correction	No Attenuation Correction	Attenuation Correction	No Attenuation Correction
$\Delta X \pm \sigma$	$2.25 \pm 0.33$	$2.30 \pm 0.33$	$3.09 \pm 0.33$	$3.13 \pm 0.33$
$\Delta Y \pm \sigma$	$3.29 \pm 0.23$	$3.24 \pm 0.23$	$4.82 \pm 0.22$	$4.81 \pm 0.22$

### 5.2.3.3 Triple-Line Source Phantom

Figure 36 shows the PET/CT alignment test results for the Triple-Line Source phantom. Table 25 provides the measured alignment errors for the different PET/CT acquisitions. The alignment errors using the 2D acquisitions are larger than the errors using 3D acquisitions. Similar to the Manual method and the Maximum-Pixel Value method, the Curve-fitting method gave smaller errors with smaller uncertainties.

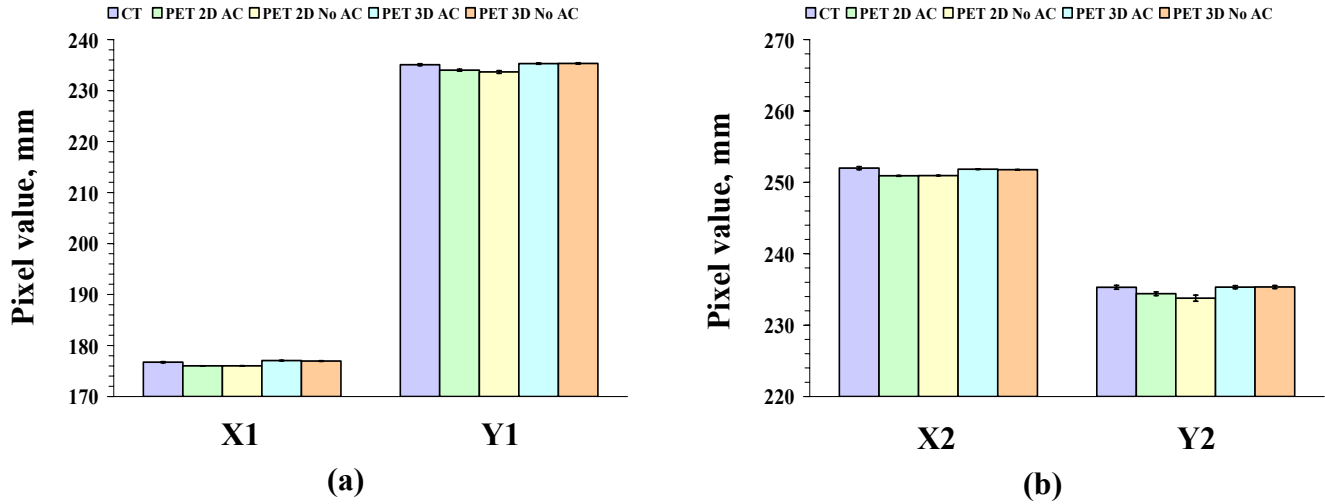


Figure 36: Measured center coordinates using the Curve-fitting method for the triple line source phantom without rotation for (a) first source and (b) second source.

Table 25: Measured PET/CT alignment errors for the triple line source phantom using the Curve-fitting method

Sources	Alignment error (mm)	2D		3D	
		Attenuation Correction	No Attenuation Correction	Attenuation Correction	No Attenuation Correction
Source 1	$\Delta X1 \pm \sigma$	$0.74 \pm 0.04$	$0.74 \pm 0.04$	$0.34 \pm 0.04$	$0.23 \pm 0.04$
	$\Delta Y1 \pm \sigma$	$1.10 \pm 0.08$	$1.46 \pm 0.10$	$0.22 \pm 0.07$	$0.25 \pm 0.07$
Source 2	$\Delta X2 \pm \sigma$	$1.10 \pm 0.07$	$1.06 \pm 0.06$	$0.15 \pm 0.06$	$0.22 \pm 0.06$
	$\Delta Y2 \pm \sigma$	$0.93 \pm 0.12$	$1.56 \pm 0.16$	$0.02 \pm 0.11$	$0.04 \pm 0.11$
Source 3	$\Delta X3 \pm \sigma$	NA	NA	NA	NA
	$\Delta Y3 \pm \sigma$	NA	NA	NA	NA
Average	$\Delta \bar{X} \pm \sigma$	$0.92 \pm 0.04$	$0.90 \pm 0.04$	$0.24 \pm 0.04$	$0.22 \pm 0.04$
	$\Delta \bar{Y} \pm \sigma$	$1.02 \pm 0.07$	$1.51 \pm 0.09$	$0.12 \pm 0.06$	$0.14 \pm 0.06$

NA: not available because of the air bubble in the third insert of the Triple-Line Source phantom while acquiring the PET images

### 5.2.3.4 Triple-Line Source Phantom Rotated by 45°

Figure 37 gives the PET/CT alignment test data obtained for the Triple-Line Source phantom rotated by 45°. Table 26 provides the measured alignment errors for different PET/CT acquisitions. The average x-coordinate error is considerably smaller than the average y-coordinate error for both the acquisitions. Again, of all acquisitions, 3D acquisitions gave larger alignment errors.

Table 26: Measured PET/CT alignment errors for the triple line source phantom rotated by 45° using the Curve-fitting method

Sources	Alignment error (mm)	2D		3D	
		Attenuation Correction	No Attenuation Correction	Attenuation Correction	No Attenuation Correction
Source 1	$\Delta X1 \pm \sigma$	$0.28 \pm 0.13$	$0.18 \pm 0.13$	$1.54 \pm 0.16$	$1.19 \pm 0.16$
	$\Delta Y1 \pm \sigma$	$1.36 \pm 0.03$	$1.41 \pm 0.03$	$2.63 \pm 0.04$	$2.67 \pm 0.04$
Source 2	$\Delta X2 \pm \sigma$	$0.12 \pm 0.13$	$0.12 \pm 0.13$	$1.17 \pm 0.16$	$1.03 \pm 0.16$
	$\Delta Y2 \pm \sigma$	$1.80 \pm 0.08$	$1.78 \pm 0.08$	$2.89 \pm 0.06$	$2.86 \pm 0.06$
Source 3	$\Delta X3 \pm \sigma$	NA	NA	NA	NA
	$\Delta Y3 \pm \sigma$	NA	NA	NA	NA
Average	$\Delta \bar{X} \pm \sigma$	$0.20 \pm 0.09$	$0.15 \pm 0.09$	$1.35 \pm 0.11$	$1.11 \pm 0.11$
	$\Delta \bar{Y} \pm \sigma$	$1.58 \pm 0.04$	$1.60 \pm 0.04$	$2.76 \pm 0.04$	$2.77 \pm 0.04$

NA: not available because of the air bubble in the third insert of the Triple-Line Source phantom while acquiring the PET images

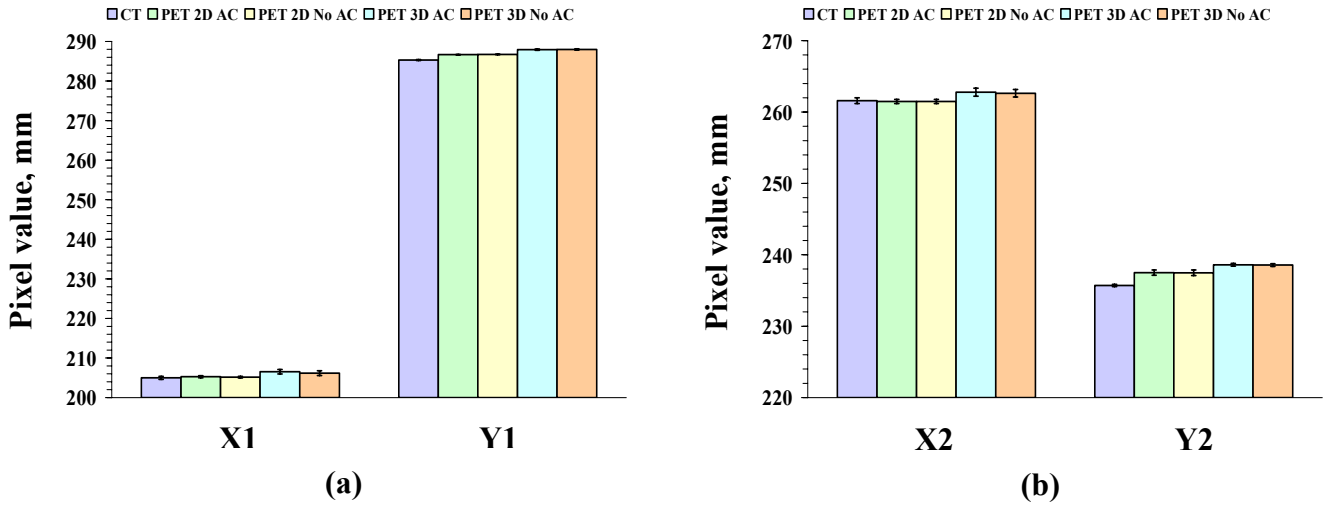


Figure 37: Measured center coordinates using the Curve-fitting method for the triple line source phantom rotated by  $45^\circ$  for (a) first source and (b) second source.

### 5.2.3.5 Hot Sphere Phantom

Figure 38 shows PET/CT alignment test results obtained using the Manual method for the Hot Sphere phantom. Table 27 provides the measured alignment errors for the different PET/CT acquisitions. The alignment errors measured using this method for the Hot Sphere phantom were substantially worse compared to the errors measured using the other methods for this phantom. The alignment errors measured for source of smallest diameter were larger and comparable to the errors for the other sources.

### 5.2.4 Summary of PET/CT Alignment Test Results

PET/CT alignment test results measured using the three analyzing methods explained in the methods chapters for the modified Gammex phantom with acrylic insert are summarized as shown in the Figure 39. All the three methods have given similar results using the modified Gammex phantom with acrylic insert. The Curve-fitting

method gave the least uncertainties using these phantoms where as the Manual method and the Maximum-Pixel Value methods gave similar alignment errors and uncertainties. It is observed that 3D acquisitions gave larger errors than the 2D acquisitions using all the methods.

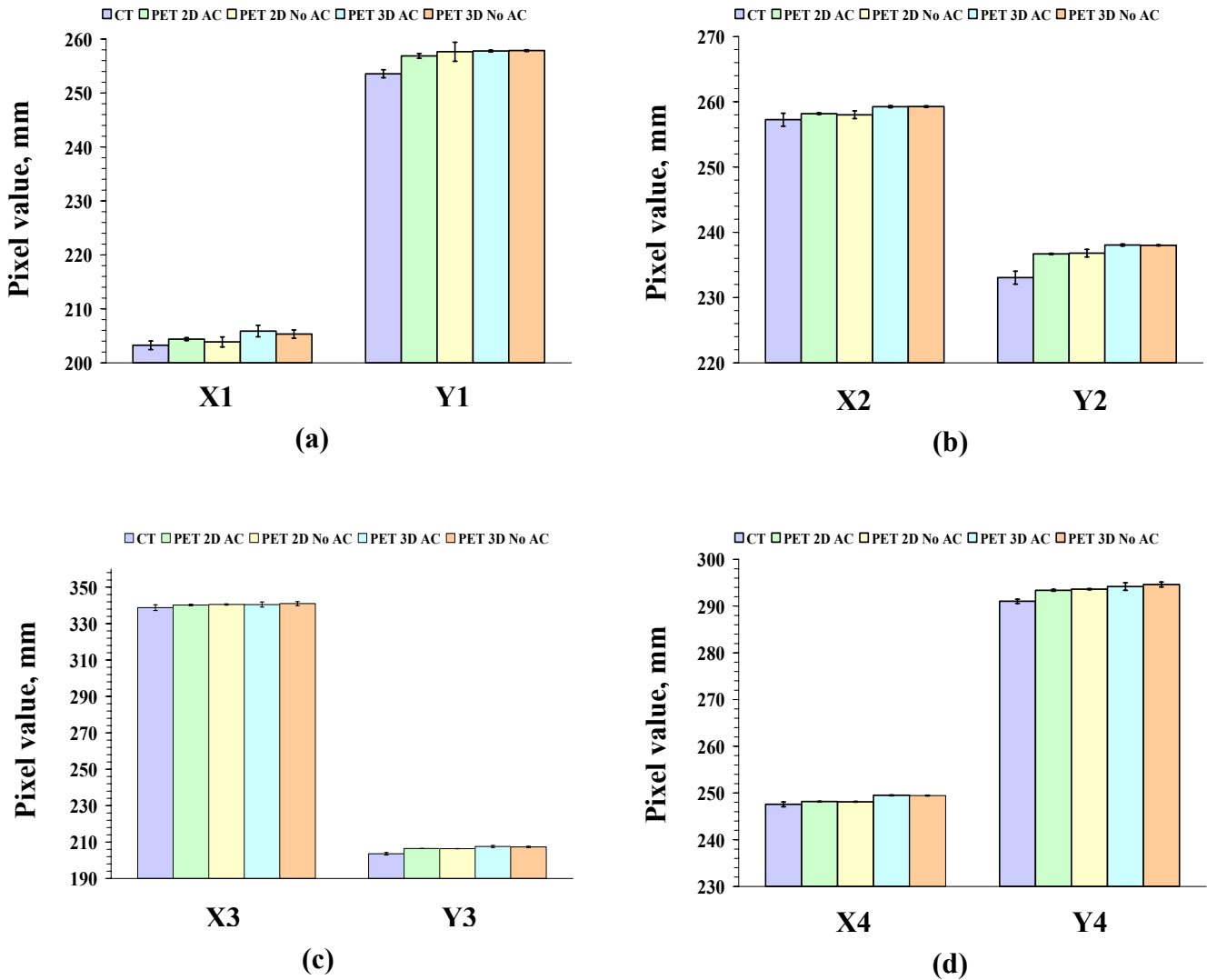


Figure 38: Measured center coordinates using the Curve-fitting method for the hot sphere phantom for (a) 18 mm diameter sphere, (b) 12 mm diameter sphere, (c) 6 mm diameter sphere, and (d) 8 mm diameter sphere.

Table 27: Measured PET/CT alignment errors for the hot sphere phantom using the Curve-fitting method

Diameter of sphere (mm)	Alignment error (mm)	2D		3D	
		Attenuation Correction	No Attenuation Correction	Attenuation Correction	No Attenuation Correction
18	$\Delta X1 \pm \sigma$	$1.15 \pm 0.21$	$0.63 \pm 0.40$	$2.64 \pm 0.44$	$2.08 \pm 0.39$
	$\Delta Y1 \pm \sigma$	$3.31 \pm 0.23$	$4.09 \pm 0.69$	$4.22 \pm 0.18$	$4.31 \pm 0.18$
12	$\Delta X2 \pm \sigma$	$0.93 \pm 0.23$	$0.75 \pm 0.29$	$1.99 \pm 0.23$	$2.02 \pm 0.23$
	$\Delta Y2 \pm \sigma$	$3.65 \pm 0.23$	$3.75 \pm 0.29$	$5.00 \pm 0.23$	$4.95 \pm 0.23$
6	$\Delta X3 \pm \sigma$	$1.43 \pm 0.40$	$1.72 \pm 0.39$	$1.71 \pm 0.67$	$2.22 \pm 0.60$
	$\Delta Y3 \pm \sigma$	$2.91 \pm 0.16$	$2.83 \pm 0.16$	$4.01 \pm 0.28$	$3.74 \pm 0.23$
8	$\Delta X4 \pm \sigma$	$0.59 \pm 0.16$	$0.55 \pm 0.17$	$1.93 \pm 0.16$	$1.87 \pm 0.16$
	$\Delta Y4 \pm \sigma$	$2.36 \pm 0.16$	$2.59 \pm 0.15$	$3.17 \pm 0.34$	$3.59 \pm 0.31$
Average	$\Delta \bar{X} \pm \sigma$	$1.03 \pm 0.17$	$0.91 \pm 0.20$	$2.07 \pm 0.25$	$2.05 \pm 0.23$
	$\Delta \bar{Y} \pm \sigma$	$3.06 \pm 0.14$	$3.32 \pm 0.23$	$4.10 \pm 0.16$	$4.15 \pm 0.15$

Figure 40 provides the summary of PET/CT alignment test results for the modified Gammex phantom with solid water insert using the three methods. It is observed that the Manual method and the Maximum-Pixel Value method gave comparable results as that of the modified Gammex phantom with acrylic results but the results obtained with Curve-fitting method for this phantom gave larger errors than the modified Gammex phantom with acrylic insert. Also, the Maximum-Pixel Value method gave large uncertainties for this phantom.

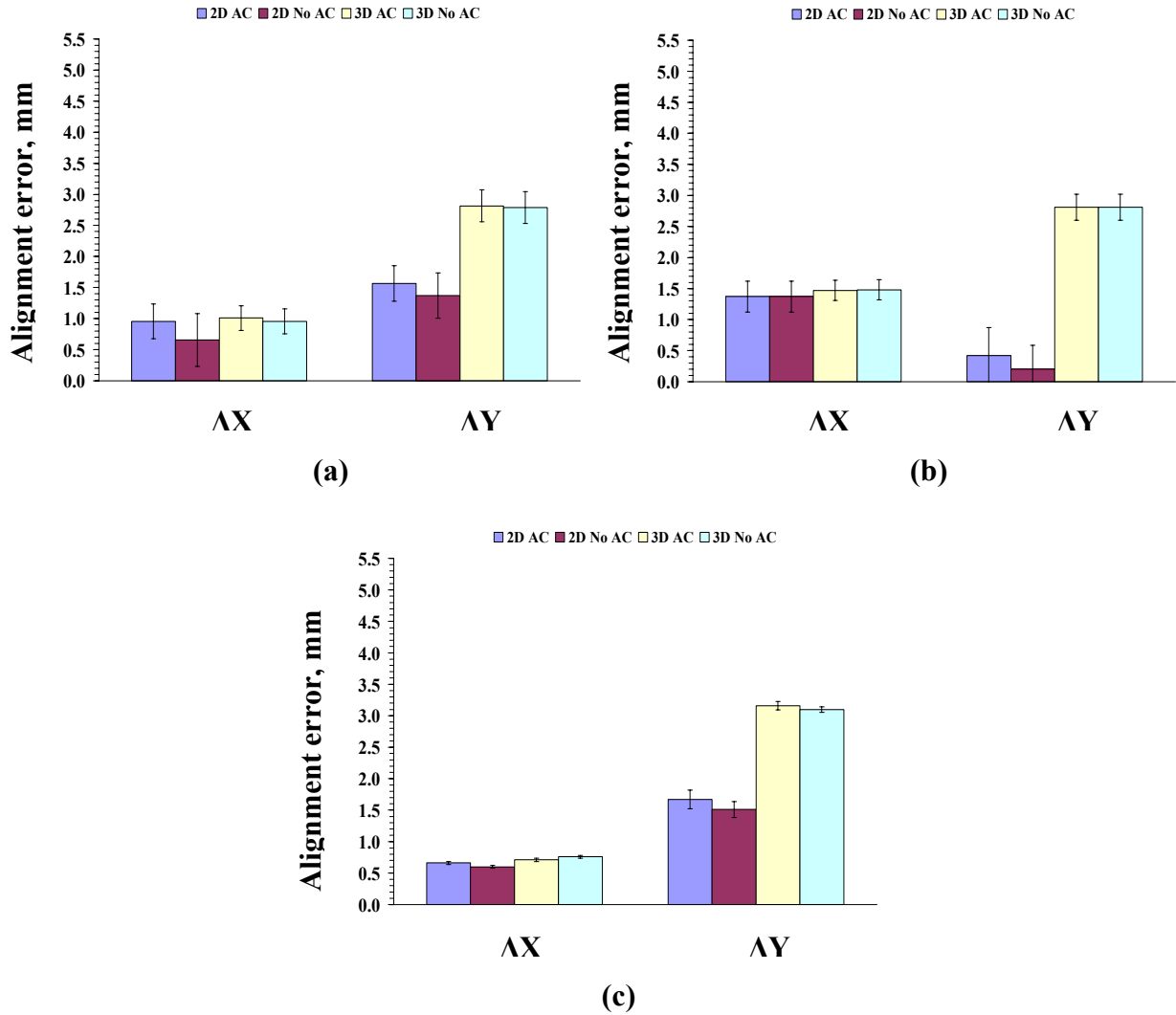


Figure 39: Measured alignment errors for the modified Gammex phantom with acrylic insert using (a) the Manual method, (b) the Maximum-Pixel Value method, and (c) the Curve-fitting method.

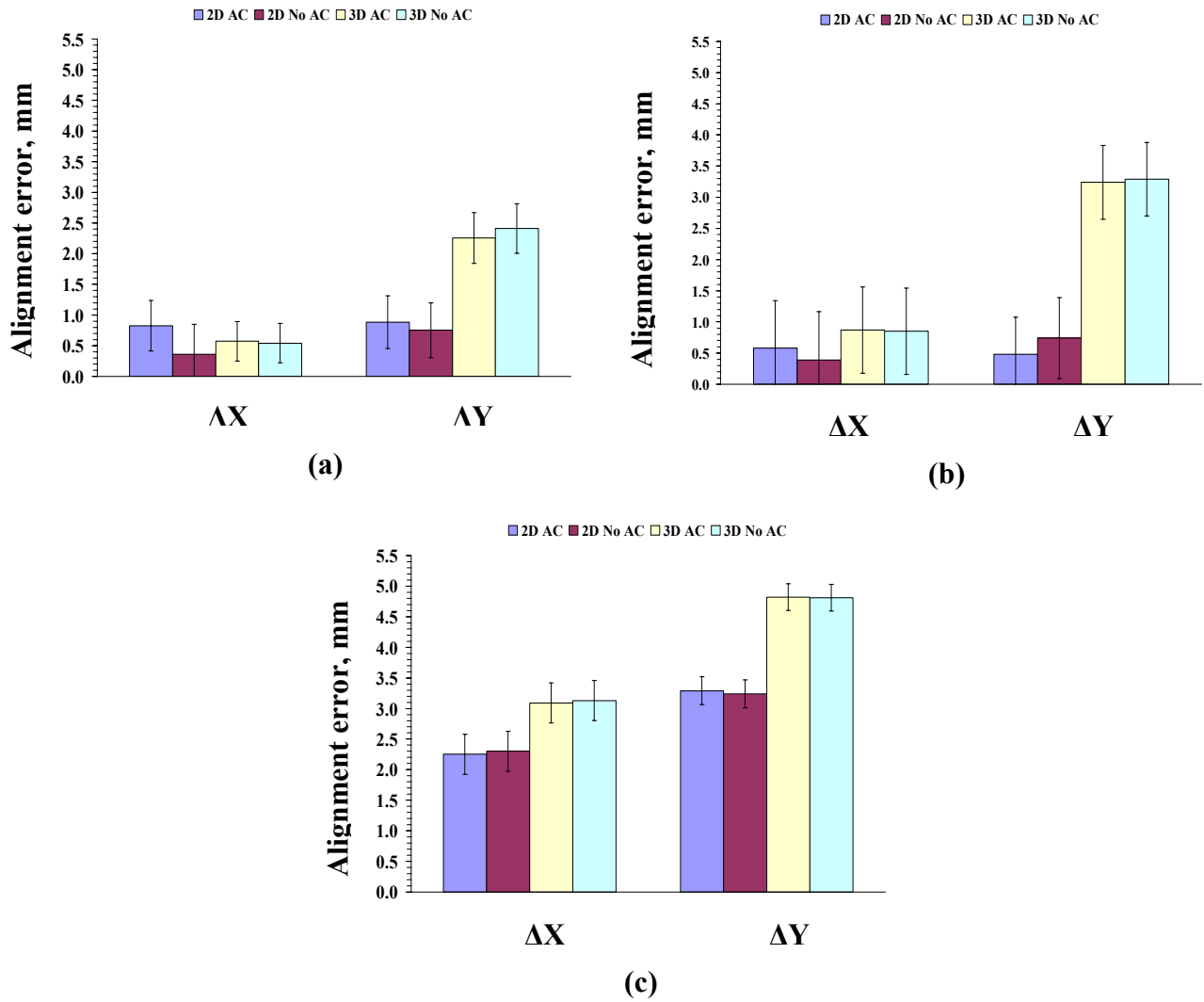


Figure 40: Measured alignment errors for the modified Gammex phantom with solid water insert using (a) the Manual method, (b) the Maximum-Pixel Value method, and (c) the Curve-fitting method.

PET/CT alignment test results for the Triple-Line Source phantom using the three methods is summarized and shown in Figure 41. As it is expected, all the three methods gave the least alignment errors with smaller uncertainties for this phantom. The Maximum-Pixel Value method gave larger alignment errors in the y-coordinates using this phantom for 3D acquisitions.

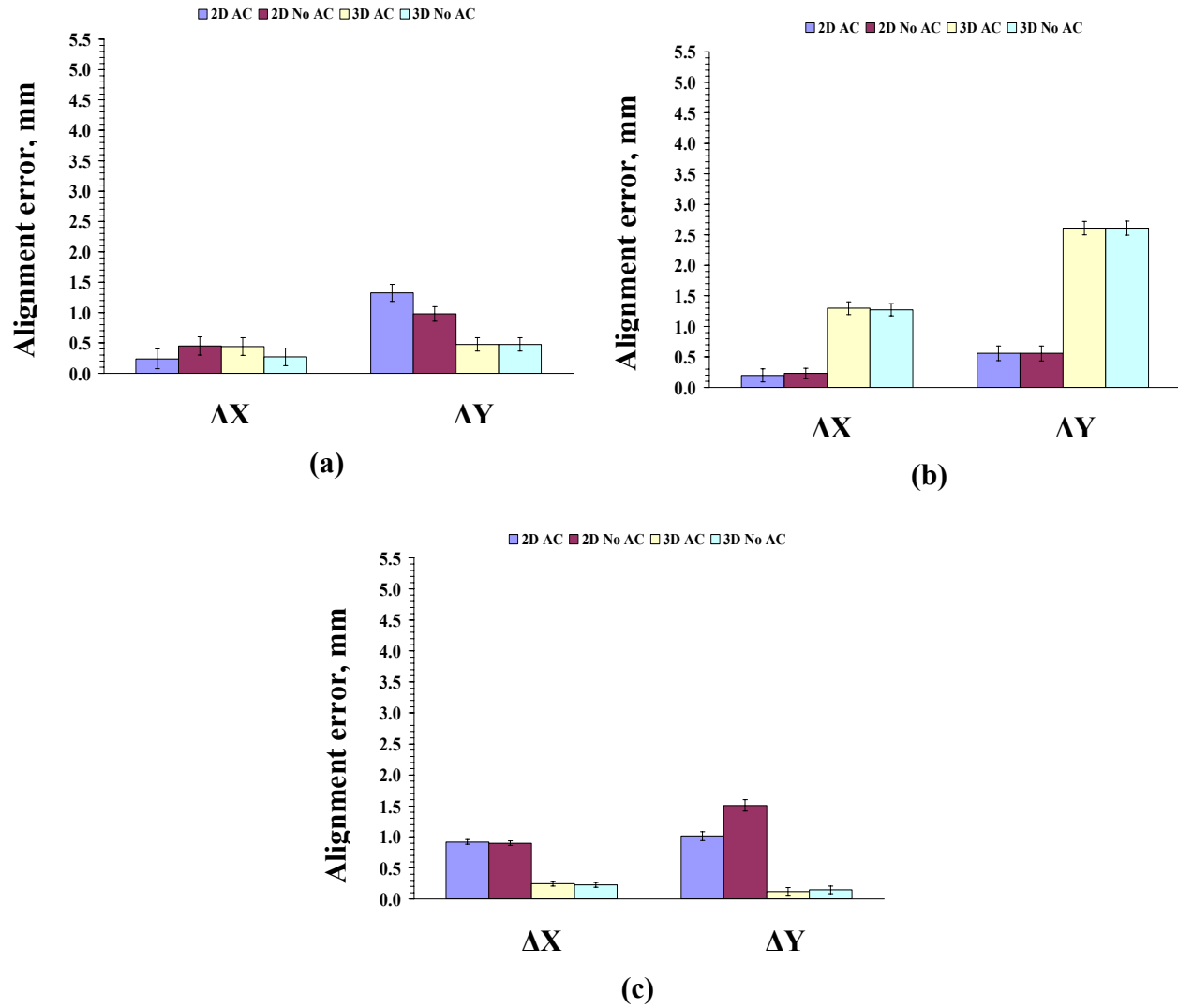


Figure 41: Measured alignment errors for the Triple-line Source phantom using (a) the Manual method, (b) the Maximum-Pixel Value method, and (c) the Curve-fitting method.

Figure 42 provides the PET/CT alignment test results measured for the Hot Sphere phantom using the three analyzing methods. All the three methods gave similar alignment errors in the x-coordinate except that of the Maximum-Pixel Value method which gave larger uncertainties. The Curve-fitting method gave larger alignment errors in the y-coordinate than the other two methods.

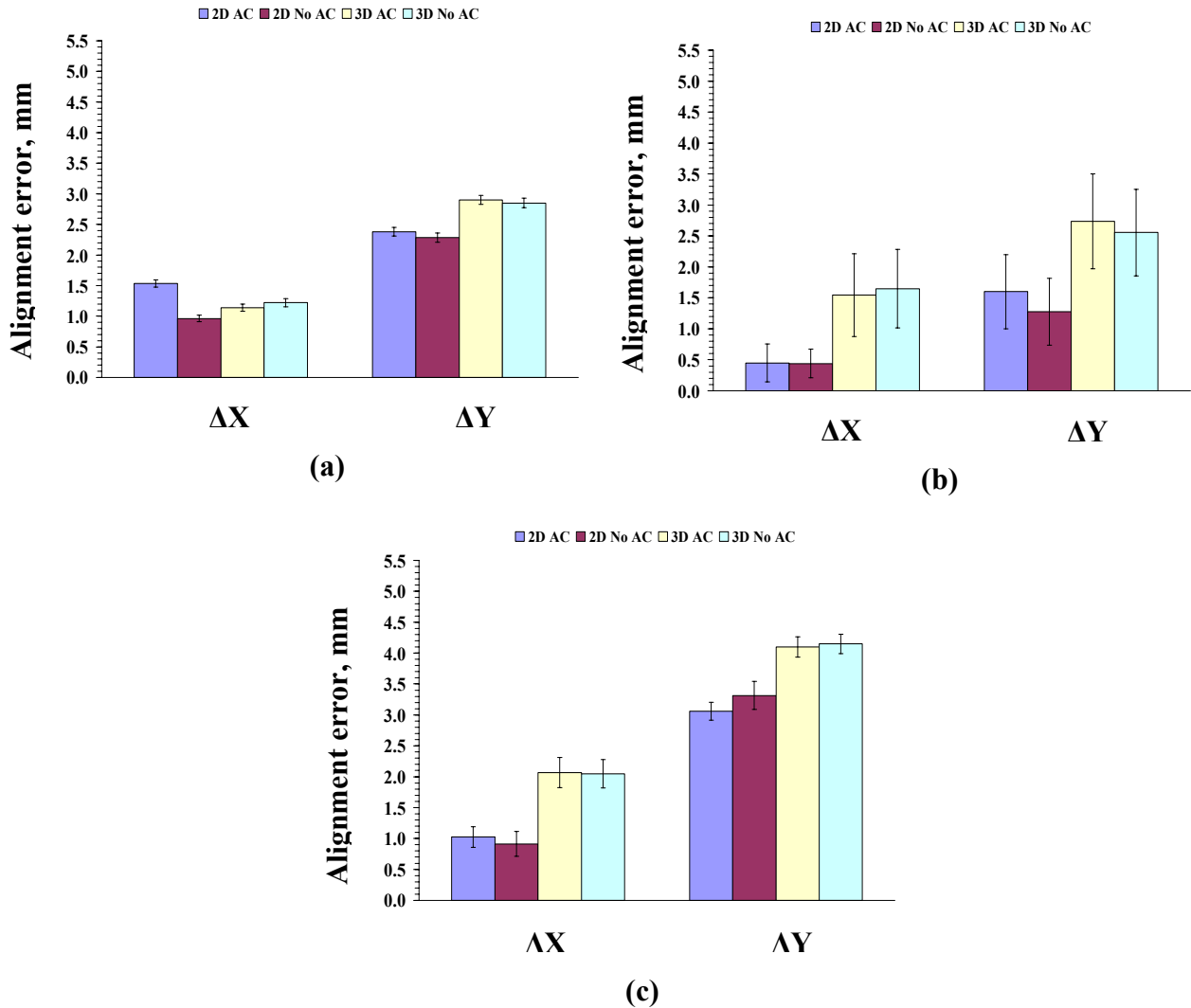


Figure 42: Measured alignment errors for the Hot Sphere phantom using (a) the Manual method, (b) the Maximum-Pixel Value method, and (c) the Curve-fitting method.

### 5.3 PET Resolution

Table 28 provides the nominal sizes and the average measured FWHM sizes in millimeters for the objects of the different phantoms. Figure 43 presents the measured FWHM sizes for each object in the different phantoms obtained from the Curve-fitting method. The 3D acquisitions produce larger apparent object sizes than the 2D acquisitions, indicating 3D resolution is worse than 2D resolution. In theory, the 1-mm

diameter line sources should provide the most accurate resolution measurement. However, the measured size of the line sources is somewhat larger than one would expect from the manufacturer's specifications for this scanner. The measured sizes for the largest spheres are actually smaller than the nominal object size, which seems incongruous. The results for the 6-mm and 8-mm diameter objects, however, seem more consistent with an expected resolution of ~5 mm FWHM. For instance, for the 8-mm cavity of the acrylic insert, an estimate of PET resolution is given from Equation 3 (p.29) as

$$\sqrt{(9.5\text{mm})^2 - (8\text{mm})^2} = 5.1 \text{ mm} \quad (\text{Equation 4})$$

A possible explanation is that an iterative reconstruction algorithm was used to reconstruct the PET images, rather than filtered backprojection. Filtered backprojection is usually recommended for doing resolution measurements; however, for routine QC, one should use the reconstruction method commonly used for patient data, which is iterative reconstruction in this case. Depending on the implementation of the iterative algorithm, the reconstructed images could be converging to produce apparently similar object sizes for the different objects. Further investigation of this behavior is probably warranted, particularly if one hopes to use PET data in conjunction with CT data to help with drawing tumor boundaries for treatment planning.

Table 28: Average measured object size for different phantoms using the Curve-fitting method to determine the resolution

Phantom	Object size (diameter)	Average measured object size (FWHM)
Acrylic insert	8 mm	9.5 mm
Solid water insert	8 mm	9.45 mm
Triple-line source phantom	1 mm	7.2 mm
Hot sphere phantom	6 mm	7.8 mm
	8 mm	9.24 mm
	12 mm	8.57 mm
	18 mm	11.58 mm

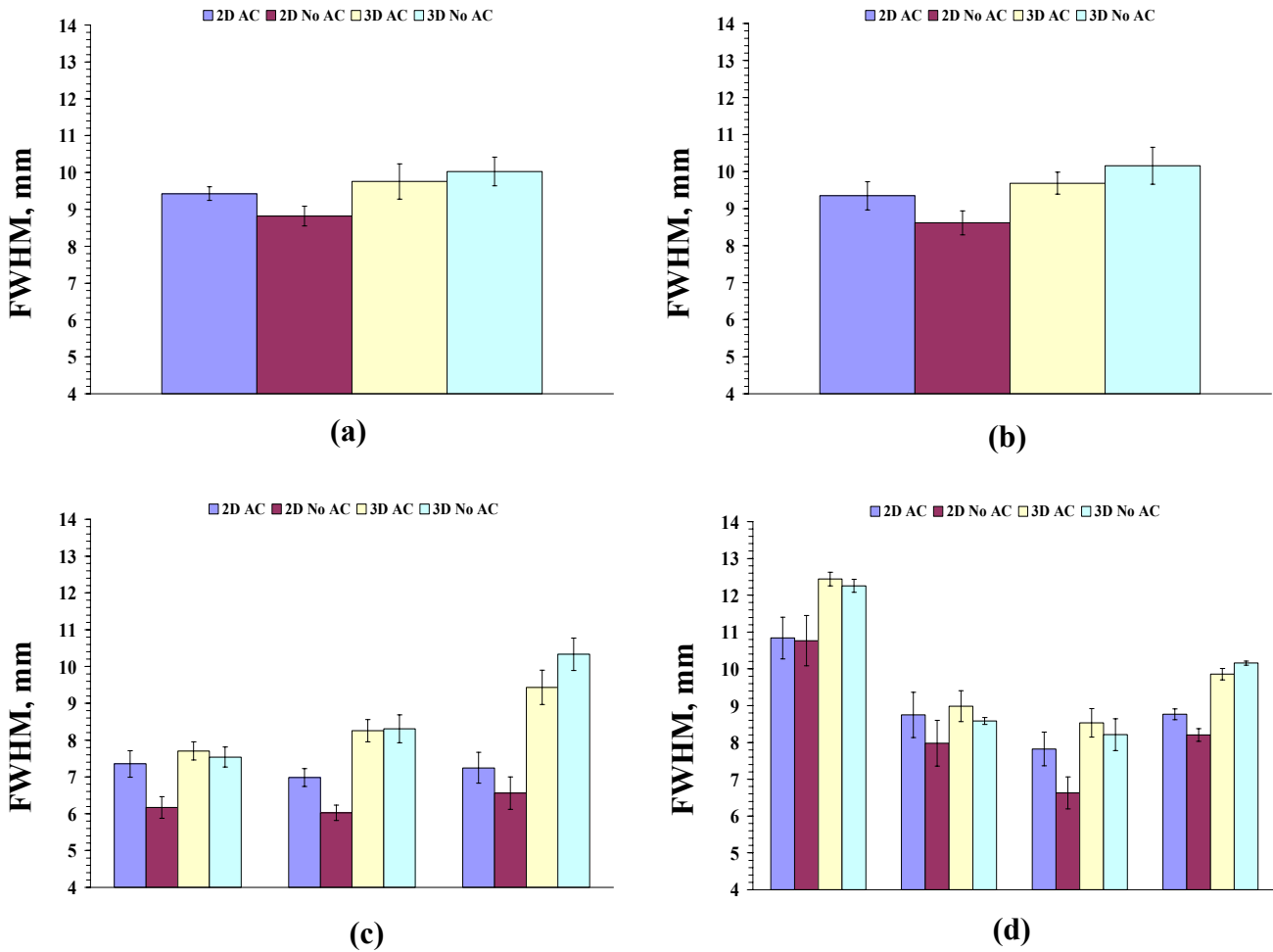


Figure 43: Measured FWHM for (a) modified Gammex phantom with acrylic insert, (b) modified Gammex phantom with solid water insert, (c) triple line source phantom with center bars representing the line source at the center, and (d) hot sphere phantom with spheres of diameters 18 mm, 12 mm 6 mm and 8 mm respectively.

## CHAPTER 6

### SUMMARY AND CONCLUSIONS

The primary purpose of this study was to determine if a CT QA phantom could be modified to allow assessment of PET/CT alignment, without altering the quality of CT QA results. The Gammex 464 CT QA phantom was modified to allow the insertion of a radioactive PET marker. The phantom was evaluated for its ability to measure PET/CT alignment and PET resolution in addition to its routine CT quality assurance testing. Two dedicated radioisotope imaging phantoms were also evaluated for PET/CT alignment QA.

CT quality assurance tests were performed on the unmodified Gammex phantom using the ACR-recommended methods. Then these tests were performed on the modified Gammex phantom. The CT QA results were compared to check for the impact of modification on the QA tests. We observed that the modification had little impact on CT QA results. The modified Gammex phantoms with acrylic insert and solid water insert gave similar results as the unmodified phantom. A summary of the results obtained for different CT parameters using the three different Gammex phantoms is provided in Table 29. Except for the CT number calibration of acrylic in the unmodified phantom, which was slightly out of range, the results were within the range prescribed in the Instruction Manual for the Gammex phantom.

PET/CT alignment was measured using three methods for determining the centers of the objects in the images. Using each method, the center coordinates were obtained for the CT and PET images, and the alignment error between them was calculated. We found

that although the Manual method produced small alignment errors, the results depend on the user's capability in selecting points for drawing a profile across the source and hence detecting the center coordinates. The Manual method was difficult to use with the Gammex phantom with solid water insert because it was difficult to distinguish between the edge of the insert and the surrounding phantom material, which is also solid water. Thus using insert materials of a different density is advantageous to overcome this difficulty. The Maximum-Pixel Value method was faster than the other methods, but some skill is required in selecting the images to be analyzed. In particular, one must select images that have all sources visible. The Curve-fitting method is the least subjective method and it provides measured PET resolution as well as alignment error.

Table 29: Results obtained for different CT parameters using the three CT QA phantoms

<b>CT Parameter tested</b>	<b>Unmodified Gammex Phantom</b>	<b>Modified Gammex Phantom with acrylic Insert</b>	<b>Modified Gammex Phantom with solid water insert</b>
CT number calibration	CT number for acrylic slightly out of range	All materials within the given range	All materials within the given range
Slice Thickness (2.5 mm, 5 mm, 7.5 mm at 120 kVp)	2.75 mm, 5 mm, 7.25 mm at 120 kVp	2.5 mm, 5 mm, 7.5 mm at 120 kVp	2.5 mm, 5 mm, 7.5 mm at 120 kVp
Low contrast resolution	6 mm cylinders visible	6 mm cylinders visible	6 mm cylinders visible
High Contrast resolution	7 lp/cm visible	7 lp/cm visible	7 lp/cm visible
Uniformity	2 HU	3 HU	2 HU

The results using the Manual method for the Gammex phantom with the solid water insert and the acrylic insert gave comparable results. But, considering the difficulty

in using the modified Gammex phantom with the solid water insert, the modified Gammex phantom with the acrylic insert is the better choice for this method. Also, the triple line source phantom without any rotation gave smaller errors compared to the other phantoms using the Manual method. The results using the Maximum-Pixel Value method for the modified Gammex phantom with solid water insert gave less error than the other phantoms using this method but it also gave large uncertainties of these errors. Using the Curve-fitting method gave worse results for all the phantoms other than the Triple-line Source phantom and the modified Gammex phantom with acrylic insert when compared to the other methods. Considering the amount of time consumed for getting the results using the Manual method, the Maximum-Pixel Value method is a better routine choice as it is faster than the other methods. Also, considering the difficulties in using the solid water insert for the modified Gammex phantom, the modified Gammex phantom with the acrylic insert is a better choice for measuring PET/CT alignment errors.

In the future, obtaining a solid radioactive source, such as sodium 22, for the modified Gammex phantom may be desired. For a solid source, the chance of leaking of radioactive materials is minimized and a Na-22 source can be utilized for longer span of time because of the long half life of Na-22 compared to the 110-minute half-life of F-18. However, using F-18 simplifies issues such as storage of the radioactive insert between QA sessions.

For future insert designs, it is not completely clear whether making the source cavity smaller would benefit the alignment testing process. The 8-mm diameter cavity and the 6-mm and 8-mm diameter spheres gave results that seem consistent with the expected scanner resolution. On the other hand, the hot spheres data indicate that smaller

objects are preferred to larger objects. A series of tests of inserts with different cavity sizes for the radiotracer would probably be helpful to address this question.

## REFERENCES

1. Leibel SA, Phillips TL: Textbook of Radiation Oncology. Philadelphia, WB Saunders Company, 1998
2. Introduction to CT Physics.  
<http://www.fleshandbones.com/readingroom/pdf/940.pdf>
3. Introduction to Nuclear Medicine.  
[www.rah.sa.gov.au/nucmed/PET/pet\\_info.htm](http://www.rah.sa.gov.au/nucmed/PET/pet_info.htm)
4. Learning solutions from GE: Principles of PET/CT imaging. Program supplement
5. Zanzonico P: Positron emission tomography: A review of basic principles, scanner design and performance, and current systems. *Semin Nucl Med* 34:87-111, 2003
6. Hasegawa BH, Stebler B, et al: A prototype high-purity germanium detector system with fast photon-counting circuitry for medical imaging. *Med Phys* 18:900-909, 1991
7. Lang TF, Hasegawa BH, et al: Description of a prototype emission-transmission computed tomography imaging system. *J Nucl Med* 33:1881-1887, 1992
8. Keidar Z, Israel O, et al: SPECT/CT in tumor imaging: Technical aspects and clinical applications. *Semin Nuc Med* 33:205-218, 2003.
9. Labbe JP: SPECT/CT emerges from shadow of PET/CT.  
[http://www.gammamedica.com/articles/603\\_Reprint.pdf](http://www.gammamedica.com/articles/603_Reprint.pdf)
10. Townsend DW: A combined PET/CT scanner: The choices. *J Nucl Med* 42:533-534, 2001
11. Ell PJ, Von Schulthess GK: PET/CT: A new road map. *Eur J Nucl Med Mol Imaging* 29:719-720, 2002
12. Beyer T, Townsend DW, Brun T, et al: A combined PET/CT scanner for clinical oncology. *J Nucl Med* 41:1369-1379, 2000
13. Valk PE, Bailey DL, Townsend DW, Maisey MN: Positron Emission Tomography, Basic science and clinical practice. New York, Springer, 2003
14. Townsend DW, Beyer T, et al: PET/CT scanners: A hardware approach to image fusion. *Semin Nucl Med* 33:194-204, 2003

15. Chmielewski L, Kozinska D: Image Registration.  
<http://www.zssk.pwr.wroc.pl/zssk/kosyr/kosyr.html>
16. Hutton BF, Braun M, Thurfjell L, et al: Image registration: An essential tool for nuclear medicine. *Eur J Nucl Med* 29:559-577, 2002
17. Lavelly WC, Scarfone C, Cevikalp H, Li R, Byrne DW, Cmelak AJ, et al: Phantom validation of co-registration of PET and CT for image-guided radiotherapy. *Med Phys* 31:1083-1092, 2004
18. Patton JA, Delbeke D, Sandler MP: Image fusion using an integrated, dual-head coincidence camera with X-ray tube-based attenuation maps. *J Nucl Med* 41:1364-1368, 2000
19. Shrivastava P, Paliwal B, Fang Y, et al: Evaluation of CT/PET fusion images for defining tumor treatment volumes. San Diego, AAPM 45<sup>th</sup> Annual Meeting, 2003 (abstract)
20. ACR CT Accreditation phantom, Gammex 464: Testing the ACR phantom, Instruction Manual. [www.gammex.com](http://www.gammex.com)
21. Triple-line Insert for the Deluxe SPECT phantom.  
[http://www.spect.com/pub/Triple\\_Line\\_Insert.doc.pdf](http://www.spect.com/pub/Triple_Line_Insert.doc.pdf)
22. Hot Sphere phantom.  
[http://www.spect.com/pub/Hollow\\_Sphere\\_Sets.doc.pdf](http://www.spect.com/pub/Hollow_Sphere_Sets.doc.pdf)
23. Bevington PR, Robinson DK: Data Reduction and Error Analysis for the Physical Sciences. New York, McGraw-Hill, 2003

# APPENDIX A

## IDL PROGRAMS FOR MANUAL METHOD

1. This program uses a built in function PROFILE to draw profiles between the selected points for CT images.

```
pro ctt1
!p.multi[2] = 4
!p.charsize=1.5
!x.style = 3
window, 0, xsize=512, ysize=512

A=read_dicom('F:\ISGARS\1\1586')
tvsc1,A
R = PROFILE(A)
WINDOW, /FREE,0, xsize=500, ysize=500
PLOT, R

!p.multi = 0
end
```

2. This program uses a built in function PROFILE to draw profiles between the selected points for PET images

```
pro pet1
!p.multi[2] = 4
!p.charsize=1.5
!x.style = 3
window, 0, xsize=564, ysize=566

A=read_dicom('F:\ISGARS\0\272')
magnifiedImg = CONGRID(A, 614, 614, /INTERP)
C=intarr(564,566)
C=magnifiedImg[49:613,47:613]
X=MAX(C)
tvsc1,C
R = PROFILE(C)
WINDOW, /FREE,0, xsize=512, ysize=512
PLOT, R
!p.multi = 0
end
```

## APPENDIX B

### IDL PROGRAMS FOR MAXIMUM-PIXEL VALUE METHOD

1. This is the main program which uses several sub-routines such as CT\_X and CT\_Y to measure the center of the objects in a selected region given as input. X\_LOW, X\_HIGH, Y\_LOW and Y\_HIGH are given as input to describe the region of interest in the CT image. X and Y are given as input to select the range of images to be considered for analyzing.

```
pro TRIAL_ct_tisp_rotn

!p.multi[2] = 4
!p.charsize=1.5
!x.style = 3

OPENW,1,'C:\Documents and Settings\prashanth\Desktop\point.txt'
read,PROMPT='Enter X LOW  :',X_LOW
read,PROMPT='Enter X HIGH :',X_HIGH
read,PROMPT='Enter Y LOW  :',Y_LOW
read,PROMPT='Enter Y HIGH :',Y_HIGH
read,PROMPT='Enter X: ',X
read,PROMPT='Enter Y: ',Y
x=fix(x)
y=fix(y)
for i=X,Y do begin
    IMAGE='F:\ISGARS\0\'+string(i)
    words = STRSPLIT(IMAGE, ' ', /EXTRACT)
    CT_IMAGEPATH=words[0]+words[1]

printf,1,CT_IMAGEPATH, '(' ,CT_X(CT_IMAGEPATH,X_LOW,X_HIGH,Y_LOW,Y_HIGH) , '
, ',CT_Y(CT_IMAGEPATH,X_LOW,X_HIGH,Y_LOW,Y_HIGH) , '
endfor
close,1

!p.multi = 0
end
```

2. A sub-routine CT\_X is called in the main program. This sub-routine uses the inputs given in the main program and measures the center coordinates in X of the objects of interest of CT images using several built-in functions.

```

FUNCTION CT_X, IMAGEPATH, R, M, S, N
A=read_dicom(IMAGEPATH)
X=0.90*MAX(A)
for i=M,R-1,-1.0 do begin
  for j=N,S-1,-1.0 do begin
    if A[i,j] GT X then begin
      k=i
      i=10.0
      j=10.0
    ENDIF
  endfor
endfor

for i=R,M-1.0 do begin
  for j=S,N-1.0 do begin
    if A[i,j] GT X then begin
      l=i
      i=1000.0
      j=1000.0
    ENDIF
  endfor
endfor

x_CT=(1+(k-l)/2)
RETURN, x_CT
END

```

3. A sub-routine CT\_X is called in the main program. This sub-routine uses the inputs given in the main program and measures the center coordinates in Y of the objects of interest using several built-in functions.

```

FUNCTION CT_Y, IMAGEPATH, R, M, S, N
A=read_dicom(IMAGEPATH)
X=0.9*MAX(A)
for j=N,S-1,-1.0 do begin
  for i=M,R-1,-1.0 do begin
    if A[i,j] GT X then begin
      p=j
      i=10.0
      j=10.0
    ENDIF
  endfor
endfor

for j=S,N-1.0 do begin
  for i=R,M-1.0 do begin
    if A[i,j] GT X then begin
      q=j
      i=1000.0
      j=1000.0
    ENDIF
  endfor
endfor

y_CT=(q+(p-q)/2)
RETURN, y_CT
END

```

4. This is the main program which uses several sub-routines such as PET\_X and PET\_Y to measure the center of the objects in a selected region given as input. X\_LOW, X\_HIGH, Y\_LOW and Y\_HIGH are given as input to describe the region of interest in the PET image. X and Y are given as input to select the range of images to be considered for analyzing.

```

pro TRIAL_pet
!p.multi[2] = 4
!p.charsize=1.5
!x.style = 3

OPENW,1,'C:\Documents and Settings\prashanth\Desktop\proj\point.txt '
read,PROMPT='Enter X LOW  :',X_LOW
read,PROMPT='Enter X HIGH :',X_HIGH
read,PROMPT='Enter Y LOW  :',Y_LOW
read,PROMPT='Enter Y HIGH :',Y_HIGH
read,PROMPT='Enter X:',X
read,PROMPT='Enter Y:',Y
x=fix(x)
y=fix(y)

for i=X,Y do begin

    IMAGE='F:\ISGARS\0\'+'+string(i)
    words = STRSPLIT(IMAGE, ' ', /EXTRACT)
    PET_IMAGEPATH=words[0]+words[1]

printf,1,PET_IMAGEPATH, '(' ,PET_X(PET_IMAGEPATH,X_LOW,X_HIGH,Y_LOW,Y_HIGH
), ', ',PET_Y(PET_IMAGEPATH,X_LOW,X_HIGH,Y_LOW,Y_HIGH), ')'
endfor

close,1
!p.multi = 0
end

```

5. A sub-routine PET\_X is called in the main program. This sub-routine uses the inputs given in the main program and measures the center coordinates in X of the objects of interest of PET images using several built-in functions.

```

FUNCTION PET_X, IMAGEPATH, R, M, S, N
A=read_dicom(IMAGEPATH)
magnifiedImg = CONGRID(A, 614, 614, /INTERP)
C=intarr(564,566)
C=magnifiedImg[49:613,47:613]
X=0.60*MAX(C)

for i=M,R-1,-1.0 do begin
    for j=N,S-1,-1.0 do begin
        if C[i,j] GT X then begin

```

```

        k=i
        i=10.0
        j=10.0
        ENDIF
    endfor
endfor

for i=R,M-1.0 do begin
    for j=S,N-1.0 do begin
        if C[i,j] GT X then begin
            l=i
            i=1000.0
            j=1000.0
            ENDIF
        endfor
    endfor

x_PET_256=(1+(k-1)/2)
RETURN,x_PET_256
END

```

6. A sub-routine PET\_X is called in the main program. This sub-routine uses the inputs given in the main program and measures the center coordinates in Y of the objects of interest of PET images using several built-in functions.

```

FUNCTION PET_Y,IMAGEPATH,R,M,S,N
A=read_dicom(IMAGEPATH)
magnifiedImg = CONGRID(A, 614, 614, /INTERP)
C=intarr(564,566)
C=magnifiedImg[49:613,47:613]
X=0.60*MAX(C)

for j=N,S-1,-1.0 do begin
    for i=M,R-1,-1.0 do begin
        if C[i,j] GT X then begin
            p=j
            i=10.0
            j=10.0
            ENDIF
        endfor
    endfor

for j=S,N-1.0 do begin
    for i=R,M-1.0 do begin
        if C[i,j] GT X then begin
            q=j
            i=1000.0
            j=1000.0
            ENDIF
        endfor
    endfor

y_PET_256=(q+(p-q)/2)
RETURN,y_PET_256
END

```

## APPENDIX C

### IDL PROGRAMS FOR CURVE-FITTING METHOD

1. This is the main program utilizing sub-routines such as `tlsp_ct_x` and `tlsp_ct_y` to evaluate the center coordinates of the objects in a selected region given by `X_LOW`, `X_HIGH`, `Y_LOW` and `Y_HIGH` values. The range of images to be considered for the analysis is given by `X` and `Y` values.

```
PRO tlsp_ct_fit
!p.multi[2] = 4
!p.charsize=1.5
!x.style = 3

OPENW,2,'C:\Documents and Settings\prashanth\Desktop\point1.txt'
read,PROMPT='Enter X LOW  :',X_LOW
read,PROMPT='Enter X HIGH :',X_HIGH
read,PROMPT='Enter Y LOW  :',Y_LOW
read,PROMPT='Enter Y HIGH :',Y_HIGH
read,PROMPT='Enter X:',X
read,PROMPT='Enter Y:',Y
x=fix(x)
y=fix(y)

for i=X,Y do begin
    IMAGE='F:\ISGARS\0\'+string(i)
    words = STRSPLIT(IMAGE, ' ', /EXTRACT)
    CT_IMAGEPATH=words[0]+words[1]
    printf,2,CT_IMAGEPATH, '(' ,tlsp_ct_x(CT_IMAGEPATH,x_low,x_high,y_low,y_high),tlsp_ct_y(CT_IMAGEPATH,x_low,x_high,y_low,y_high), ')'
endfor

close,2
!p.multi = 0
end
```

2. This subroutine uses the several built-in and custom made functions for analyzing the center coordinates of the objects of CT images.

```
function tlsp_ct_x,ct_imagepath,x_low,x_high,y_low,y_high
A=read_dicom(ct_imagepath)

mask12=mask_tlsp_new(x_low)
m=0.0
n=0.0
difference=fltarr(12,12)

for m=x_low,x_high do begin
    for n=y_low,y_high do begin
```

```

        for i=0,11 do begin
            for j=0,11 do begin
                difference[i,j]=mask12[i,j]-A[m+i,n+j]
            endfor
        endfor
        avg=average1(difference)
        if(avg lt 5.0)and(avg gt -5.0) then begin
;         if(avg eq 0.0) then begin
            x=m+6.0
            y=n+6.0
            m=1000.0
            n=1000.0
        endif
    endfor
endfor

return,x
end

```

3. This subroutine uses the several built-in and custom made functions for analyzing the center coordinates of the objects of PET images.

```

function tlsp_ct_y,ct_imagepath,x_low,x_high,y_low,y_high
A=read_dicom(ct_imagepath)
mask12=mask_tlsp_new(x_low)
m=0.0
n=0.0
difference=fltarr(12,12)

for m=x_low,x_high do begin
    for n=y_low,y_high do begin
        for i=0,11 do begin
            for j=0,11 do begin
                difference[i,j]=mask12[i,j]-A[m+i,n+j]
            endfor
        endfor
        avg=average1(difference)
        if(avg lt 5.0)and(avg gt -5.0) then begin
;         if(avg eq 0.0) then begin
            x=m+6.0
            y=n+6.0
            m=1000.0
            n=1000.0
        endif
    endfor
endfor

return,y
end

```

4. This subroutines creates a square template, MASK, of equal pixel values similar to the objects in the triple-line source phantom.

```

function MASK_tlsp_new,x_low
p=x_low
;OPENW,1,'C:\Documents and Settings\prashanth\Desktop\point.txt'

```

```

a=read_dicom('F:\ISGARS\0\450')
mask=fltarr(12,12)
mask[0:11,0:11]=a[174:185,236:247]
return,mask
END

```

5. This subroutine measures the average value on the array, difference, and returns this value to the `tlsp_ct_x` and `tlsp_ct_y` subroutines.

```

function average1,difference
sum=0.0
average=0.0

for i=0,11.0 do begin
    for j=0,11.0 do begin
        sum=sum+difference[i,j]
    endfor
endfor

average=sum/144.0
return,average
end

```

6. A main program, `FIT_resltn`, fits a gaussian curve to given input parameters using the subroutines `trial_fit` and `trial_fit_y` to obtain the fitted parameters which give the center coordinates of the object of interest.

```

pro FIT_resltn
!p.multi[2] = 4
!p.charsize=1.5
!x.style = 3

OPENW,1,'C:\Documents and Settings\prashanth\Desktop\point.txt'
read,PROMPT='Enter X LOW  :',X_LOW
read,PROMPT='Enter X HIGH  :',X_HIGH
;X_HIGH=X_LOW+19.0
read,PROMPT='Enter Y LOW   :',Y_LOW
read,PROMPT='Enter Y HIGH  :',Y_HIGH
;Y_HIGH=Y_LOW+19.0
read,PROMPT='Enter X:',X
read,PROMPT='Enter Y:',Y
x=fix(x)
y=fix(y)

for i=X,Y do begin

    IMAGE='F:\ISGARS\0\'+'+string(i)
    words = STRSPLIT(IMAGE, ' ', /EXTRACT)
    PET_IMAGEPATH=words[0]+words[1]

printf,1,PET_IMAGEPATH,'(',TRIAL_FIT(PET_IMAGEPATH,X_LOW,X_HIGH,Y_LOW,Y_HIGH),',',',',TRIAL_FIT_Y(PET_IMAGEPATH,X_LOW,X_HIGH,Y_LOW,Y_HIGH),')', 'FWHM',resltn(PET_IMAGEPATH,X_LOW,X_HIGH,Y_LOW,Y_HIGH)
endfor

```

```

close,1
!p.multi = 0
end

```

7. Subroutine, `resltn` utilizes the Gaussian curve fit function in the IDL and determines the value of the standard deviation as a fitted parameter which can be utilized for measuring the PET spatial resolution. This subroutine returns the value of FWHM as its result to the main program.

```

FUNCTION resltn,PET_IMAGEPATH_256,X_LOW,X_HIGH,Y_LOW,Y_HIGH
; Define the independent variable.
n = 20
x = FLOAT(INDGEN(20))
; Define the coefficients.
a = [1.0, 9.0, 0.5]
;print, 'Expected: For X Co-ordinate ', a
z = (x - a[1])/a[2] ; Gaussian variable
!P.MULTI = [0,2,2] ; set up 2x2 plot window
nterms=3
s=read_dicom(PET_IMAGEPATH_256)
;magnifiedImg = CONGRID(s, 614, 614, /INTERP)
;;C=intarr(564,566)
;C=intarr(512,512)
;;C=magnifiedImg[49:613,47:613]
;C=magnifiedImg[50:564,50:564]
b=fltarr(20)
k=0

for i=X_LOW,X_HIGH do begin
  for j=Y_LOW,Y_HIGH do begin
    b[k]=b[k]+s[i,j]
  endfor
  k=k+1
endfor

y=b
;print,y
y = y + a[0]*exp(-z^2/2)
;print,y
; Fit the data to the function, storing coefficients in
; coeff:
yfit = GAUSSFIT(x, y, coeff, NTERMS=nterms)
;print, 'Result:FOR X ', coeff[0:nterms-1]
; Plot the original data and the fitted curve:
;window, 0, xsize=800, ysize=500
;PLOT, x, y, TITLE='nterms='+STRTRIM(nterms,2),color=255*256L
;window, 1, xsize=800, ysize=400
;OPLOT, x, yfit, THICK=2

RETURN,coeff[2]*2.3548
End

```

8. Subroutine, `trial_fit` utilizes the Gaussian curve fit function in the IDL and determines the value of the standard deviation as a fitted parameter which can be utilized for measuring the center coordinates in X of the objects in the PET images.

```

FUNCTION trial_fit,PET_IMAGEPATH_256,X_LOW,X_HIGH,Y_LOW,Y_HIGH
; Define the independent variable.
n = 20
x = FLOAT(INDGEN(20))
; Define the coefficients.
a = [1.0, 9.0, 0.5]
;print, 'Expected: For X Co-ordinate ', a
z = (x - a[1])/a[2] ; Gaussian variable
!P.MULTI = [0,2,2] ; set up 2x2 plot window
nterms=3
s=read dicom(PET_IMAGEPATH_256)
;magnifiedImg = CONGRID(s, 614, 614, /INTERP)
;;C=intarr(564,566)
;C=intarr(512,512)
;;C=magnifiedImg[49:613,47:613]
;C=magnifiedImg[50:564,50:564]
b=fltarr(20)
k=0

for i=X_LOW,X_HIGH do begin
    for j=Y_LOW,Y_HIGH do begin
        b[k]=b[k]+s[i,j]
    endfor
    k=k+1
endfor

y=b
;print,y
y = y + a[0]*exp(-z^2/2)
;print,y
; Fit the data to the function, storing coefficients in
; coeff:
yfit = GAUSSFIT(x, y, coeff, NTERMS=nterms)
;print, 'Result:FOR X ', coeff[0:nterms-1]
; Plot the original data and the fitted curve:
;window, 0, xsize=800, ysize=500
;PLOT, x, y, TITLE='nterms='+STRTRIM(nterms,2),color=255*256L
;window, 1, xsize=800, ysize=400
;OPLOT, x, yfit, THICK=2

RETURN,coeff[1]+X_LOW
End

```

9. Subroutine, `trial_fit` utilizes the Gaussian curve fit function in the IDL and determines the value of the standard deviation as a fitted parameter which can be utilized for measuring the center coordinates in Y of the objects in the PET images.

```

FUNCTION trial_fit_y,PET_IMAGEPATH_256,X_LOW,X_HIGH,Y_LOW,Y_HIGH
; Define the independent variable.
n = 20
x = FLOAT(INDGEN(20))
; Define the coefficients.
a = [1.0, 10.0, 0.5]
;print, 'Expected: For X Co-ordinate ', a
z = (x - a[1])/a[2] ; Gaussian variable
!P.MULTI = [0,2,2] ; set up 2x2 plot window
nterms=3
s=read_dicom(PET_IMAGEPATH_256)
;magnifiedImg = CONGRID(s, 614, 614, /INTERP)
;;C=intarr(564,566)
;C=intarr(512,512)
;;C=magnifiedImg[49:613,47:613]
;C=magnifiedImg[50:564,50:564]
b=fltarr(20)
k=0

for j=y_low,y_high do begin
  for i=x_low,x_high do begin
    b[k]=b[k]+s[i,j]
  endfor
  k=k+1
endfor

y=b
;print,y
y = y + a[0]*exp(-z^2/2)
;print,y
; Fit the data to the function, storing coefficients in
; coeff:
yfit = GAUSSFIT(x, y, coeff, NTERMS=nterms)
;print, 'Result: ', coeff[0:nterms-1]
; Plot the original data and the fitted curve:
;window, 0, xsize=800, ysize=500
;PLOT, x, y, TITLE='nterms='+STRTRIM(nterms,2),color=255*256L
;window, 1, xsize=800, ysize=400
;OPLOT, x, yfit, THICK=2

RETURN,coeff[1]+Y_LOW
End

```

10. This subroutine creates a square template of same pixel value as that of spherical object 4 of the Hot Sphere phantom.

```

function MASK_spheres_4,x_low
a=x_low
point4=fltarr(5,5)
point4[0,0:4]=[0,0,0,0,0]
point4[1,0:4]=[110,145,159,123,0]
point4[2,0:4]=[139,296,434,293,142]
point4[3,0:4]=[157,412,643,430,169]
point4[4,0:4]=[132,271,412,290,136]
return,point4
END

```

11. This subroutine creates a square template of same pixel value as that of spherical object 3 of the Hot Sphere phantom.

```
function MASK_spheres_3,x_low
a=x_low
point3=fltarr(7,7)
point3[0,0:6]=[0,0,0,0,0,0,0]
point3[1,0:6]=[0,0,0,123,141,120,0]
point3[2,0:6]=[0,0,145,261,316,209,117]
point3[3,0:6]=[0,107,193,451,590,356,134]
point3[4,0:6]=[0,0,170,398,531,331,134]
point3[5,0:6]=[0,0,120,202,258,193,116]
point3[6,0:6]=[0,0,0,117,134,115,0]
return,point3
END
```

12. This subroutine creates a square template of same pixel value as that of spherical object 2 of the Hot Sphere phantom.

```
function MASK_spheres_2,x_low
a=x_low
point2=fltarr(8,8)
point2[0,0:7]=[0,0,0,0,0,0,0,0]
point2[1,0:7]=[0,0,0,0,0,0,0,0]
point2[2,0:7]=[0,0,118,134,118,0,0,0]
point2[3,0:7]=[0,107,187,294,257,150,0,0]
point2[4,0:7]=[0,137,332,586,496,222,109,0]
point2[5,0:7]=[0,132,326,570,481,208,110,0]
point2[6,0:7]=[0,104,177,265,239,141,0,0]
point2[7,0:7]=[0,0,103,130,124,0,0,0]
return,point2
END
```

13. This subroutine creates a square template of same pixel value as that of spherical object 1 of the Hot Sphere phantom.

```
function MASK_spheres_1,x_low
a=x_low
point1=fltarr(6,6)
point1[0,0:5]=[0,0,0,0,0,0]
point1[1,0:5]=[101,0,0,0,0,0]
point1[2,0:5]=[168,160,118,0,0,0]
point1[3,0:5]=[410,396,190,108,0,0]
point1[4,0:5]=[558,548,241,106,0,0]
point1[5,0:5]=[331,331,176,0,0,0]
return,point1
END
```

14. This subroutine creates a square template of same pixel value as that of solid water insert of the modified Gammex phantom with solid water insert.

```

function MASK_gam_SW,x_low
a=x_low
point=fltarr(16,16)
point [0,0:15] = [10,3,-5,-9,1,5,19,17,13,7,1,7,3,-2,-9,2]
point [1,0:15] = [2,-5,-10,3,19,21,18,13,16,13,15,19,14,5,-19,-1]
point [2,0:15] = [-11,-8,10,22,29,24,18,10,17,15,19,21,16,12,-3,-4]
point [3,0:15] = [-7,2,27,23,18,19,18,7,12,15,18,26,15,13,12,-1]
point [4,0:15] = [-7,16,30,15,11,26,26,13,18,19,18,23,22,21,18,8]
point [5,0:15] = [2,15,15,12,10,31,27,17,16,16,19,20,23,19,14,12]
point [6,0:15] = [14,14,14,20,14,20,6,6,4,-1,11,18,15,13,17,22]
point [7,0:15] = [7,22,27,24,19,14,-2,6,-1,-8,6,15,9,8,18,19]
point [8,0:15] = [10,26,20,21,25,24,8,11,-4,-3,15,25,24,17,20,14]
point [9,0:15] = [6,25,17,24,25,23,11,16,5,10,22,25,27,21,17,8]
point [10,0:15] = [-11,14,17,28,21,16,21,26,19,14,17,20,28,22,14,8]
point [11,0:15] = [-13,3,15,25,23,22,32,29,22,4,10,19,26,23,15,0]
point [12,0:15] = [-12,-7,5,21,29,22,22,22,19,5,18,21,14,17,14,-2]
point [13,0:15] = [-12,-1,-1,9,22,30,21,18,20,27,24,16,8,8,0,-8]
point [14,0:15] = [9,8,-3,-1,10,23,24,20,18,24,21,6,-5,-2,0,-2]
point [15,0:15] = [3,-2,-2,-2,-6,-7,-4,9,-1,0,3,-7,-13,-4,-5,0]
return,point
END

```

15. This subroutine creates a square template of same pixel value as that of acrylic insert of the modified Gammex phantom with acrylic insert.

```

function MASK_gam_acr,x_low
a=x_low
point=fltarr(16,16)
point [0,0:15] = [7,6,15,33,68,106,131,131,129,127,104,73,54,23,2,0]
point [1,0:15] = [16,23,53,93,129,141,139,125,117,127,132,126,118,75,14,2]
point [2,0:15] = [22,56,103,125,140,137,127,130,126,129,136,133,134,117,63,10]
point [3,0:15] = [34,95,126,131,130,125,126,132,129,131,128,129,123,119,110,43]
point [4,0:15] = [64,127,129,129,135,135,125,112,107,122,129,129,110,112,133,79]
point [5,0:15] = [93,132,133,130,136,127,92,52,38,72,111,127,117,124,135,97]
point [6,0:15] = [105,124,132,128,122,89,37,4,-3,27,78,121,126,128,132,113]
point [7,0:15] = [119,126,130,129,113,72,19,-4,-2,9,50,107,117,122,134,123]
point [8,0:15] = [111,124,131,137,121,91,23,-6,-2,8,55,110,116,129,134,124]
point [9,0:15] = [83,122,138,143,135,117,64,29,24,43,88,124,124,136,133,117]
point [10,0:15] = [721,130,137,130,125,122,119,101,88,104,118,123,122,136,126,91]
point [11,0:15] = [41,113,135,124,125,124,130,129,119,127,129,127,125,137,123,66]
point [12,0:15] = [15,71,126,133,126,128,125,130,126,129,123,125,129,134,97,27]
point [13,0:15] = [12,34,86,118,130,133,129,137,138,124,112,128,126,100,37,-2]
point [14,0:15] = [3,7,31,70,103,123,124,132,131,118,112,116,88,45,0,-6]
point [15,0:15] = [-1,0,-4,11,45,78,88,106,99,82,72,57,27,13,5,1]
return,point
END

```

## VITA

Prashanth K Nookala was born in Hyderabad, India, on October 15, 1978. He attended VNRVJIET, College of Engineering, Jawaharlal Nehru Technological University, Hyderabad, Andhra Pradesh, and received a Bachelor of Engineering degree in Mechanical Engineering in July 2001. He came to United States in January 2002, and started his graduate studies in mechanical engineering at the Louisiana State University, Baton Rouge, Louisiana. During his graduate study he got interested in Medical Physics program at LSU. He joined a master's program in medical physics and health physics at LSU in August 2002. He expects to receive this degree in May 2005.